The tensor magnetic phase theory for mesoscopic volume structures of soft magnetic materials – Quasi-static and dynamic vector polarization, apparent permeability and losses – Experimental identifications of GO steel at low induction levels

Olivier Maloberti, Manar Nesser, Elias Salloum, Stéphane Panier, Jérôme Fortin, Pascal Dassonvalle, C Pineau, T Nguyen, J-P Birat, I Tolleneer

The tensor magnetic phase theory for mesoscopic volume structures of soft magnetic materials – Quasi-static and dynamic vector polarization, apparent permeability and losses – Experimental identifications of GO steel at low induction levels

OLIVIER MALOBERTI, M Nesser, E Salloum, S Panier, J Fortin, P Dassonvalle, C Pineau, T Nguyen, J-P Birat, I Tolleneer

Graphical Abstract

The Tensor Magnetic Phase Theory for mesoscopic volume structures of soft magnetic materials – Quasi-static and dynamic vector polarization, apparent permeability and losses – Experimental identifications of GO steel at low induction levels

Leave this area blank for abstract info.

O. Maloberti[1,2,*], M. Nesser[2], E. Salloum[2], S. Panier[2], J. Fortin[2], P. Dassonvalle[1,3], C. Pineau[4], T. Nguyen[5], J-P. Birat[4], I. Tolleneer[5]

[1]*ESIEE Amiens, 14 quai de la Somme, 80080 Amiens, France*
[2]*LTI Laboratory, Avenue des Facultés - Le Bailly 80 025 Amiens, France*
[3]*MIS laboratory, UPJV, 14 Quai de la Somme – 80080 Amiens, France*
[4]*IRT-M2P, 4 rue Augustin Fresnel, 57070 Metz*
[5]*CRM Group, Zone A4B, Technologiepark 922A, BE-9052 Zwijnaarde*

In this contribution, we propose to cope with the problem of soft magnetic materials heterogeneity and non-uniformity in terms of domains structure. This non-uniformity expresses itself with space variations of domains and walls geometry and characteristic properties from the bulk towards the surface. We investigate the possibility to describe and predict these changes from a mesoscopic point of view. This paper contributes to the investigations carried out on the geometry dependent magnetic behavior of soft magnetic materials.

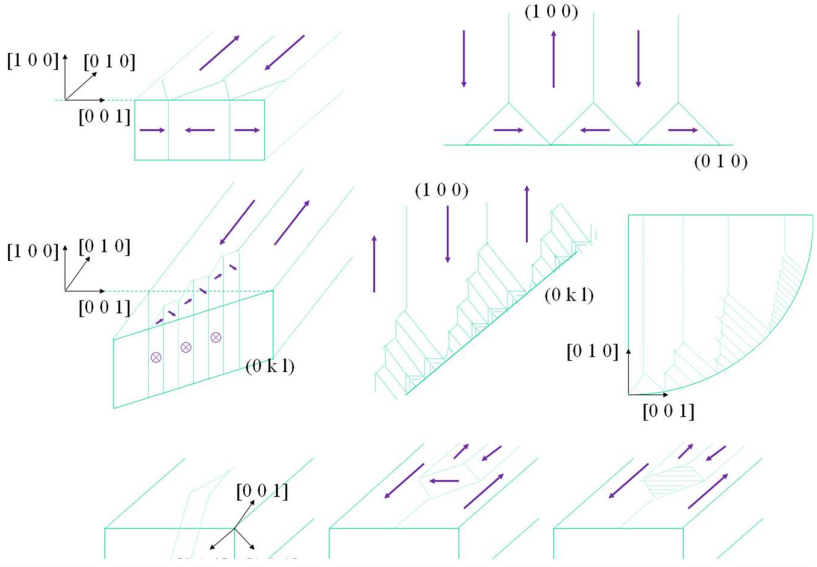

The Tensor Magnetic Phase Theory for mesoscopic volume structures of soft magnetic materials – Quasi-static and dynamic vector polarization, apparent permeability and losses – Experimental identifications of GO steel at low induction levels

O. Maloberti[1,2,*], M. Nesser[2], E. Salloum[2], S. Panier[2], J. Fortin[2], P. Dassonvalle[1,3], C. Pineau[4], T. Nguyen[5], J-P. Birat[4], I. Tolleneer[5]

[1]*ESIEE Amiens, 14 quai de la Somme, 80080 Amiens, France*
[2]*LTI Laboratory, Avenue des Facultés - Le Bailly 80 025 Amiens, France*
[3]*MIS laboratory, UPJV, 14 Quai de la Somme – 80080 Amiens, France*
[4]*IRT-M2P, 4 rue Augustin Fresnel, 57070 Metz*
[5]*CRM Group, Zone A4B, Technologiepark 922A, BE-9052 Zwijnaarde*

ARTICLE INFO

Article history:
Submitted

Keywords:
Soft Magnetic Materials
Apparent permeability
Iron Losses
Hysteresis
Domains Structures
Magnetic phases
Walls motion
Domains' magnetic rotation
Geometry and Surface Effects
Internal Tensor Variable
Exchange energy
Anisotropy energy
Demagnetization energy
Magnetostriction energy
Eddy currents

PACS: 77.80.Dj; 75; 75.10.-b; 75.60.Ch; 75.70.Kw; 75.25.Ha; 75.30.-m; 75.60.-d; 75.40.Mg; 75.47.Np.

ABSTRACT

In this contribution, we propose to cope with the problem of soft magnetic materials heterogeneity and non-uniformity in terms of domains structure. This non-uniformity expresses itself with space variations of domains and walls geometry and characteristic properties from the bulk towards the surface. We investigate the possibility to describe and predict these changes from a mesoscopic point of view. We begin with an introduction of typical subdivisions and define a tensor state variable $[\Lambda^2]$ to represent the diversity of magnetic structures with domains and walls. We then explain the material structuring thanks to an energy balance between the mesoscopic magnetic exchange, magneto-crystalline anisotropy, self-magnetostriction anisotropy, stress induced anisotropy and the dipolar demagnetizing energy. We write every contribution as a function of $[V^2]=[\Lambda^2]^{-1}$. After minimizing the total energy, we derive a formulation compatible with classical numerical methods. $[\Lambda^2]$ is deduced thanks to a partial differential equation and boundary conditions. When a time varying field is applied to the material, damping effects occur either in the volume or at the surface. Eddy currents induced within domains lead to consider a volume dissipation energy. The surface magnetic field is also damped by both the static hysteresis mainly due to defects and the dynamic hysteresis due to eddy currents around magnetic walls, added to the an-hysteretic field. The surface magnetic field, magnetic structure, and thus the polarization being known on the external surface, time variations of the volume magnetic structure can be calculated within the mass. Using the static or dynamic magnetic field coupling at the surface, the magnetic polarization can be rebuilt in the bulk to calculate the apparent magnetic permeability. Finally, finding the geometry and frequency dependent vector magnetic behavior and iron losses becomes possible. The tensor magnetic phase theory is able to account for the sensitivity of the magnetic structure to the geometry, the macroscopic anisotropy partly influenced by the metallography, the residual or induced stress, some surface effects such as the texture, the rugosity or even any scribing patterns, at mesoscopic scale. Two test cases for GO and NGO electrical steels are presented. Sensitivity analysis on the test case with GO steel are discussed. Results are then confronted to static and dynamic measurements of GO SiFe sheet samples. This paper contributes to the investigations carried out on the geometry dependent magnetic behavior of soft magnetic materials.

1. Introduction, State of The Art and Generalities

Most of existing material representations [1], even including the dynamic hysteresis and iron losses [2], ignore local microscopic non uniformities. These concern the magnetic structure (domains and walls [3]) and are mainly due to surface effects, anisotropy and exchange. This structure has its origin in the possibility of lowering the energy of a system by going from a saturated configuration with high

magnetic energy to a domains configuration, with a lower energy. The domains structure found are partially induced by the presence of the external surfaces of the crystal, and it is therefore not unexpected to find that it may be altered radically by changes in these surfaces. The size of a domain is not a fundamental length of physics, but rather sensitive to geometry and material in hand [4-7]. The microscopic scale is associated to the walls and domains; at the macroscopic scale we consider the geometry entirely. We will investigate the possibility to account for the sensitivity of the magnetic structure and its characteristic length to the macroscopic geometry at an intermediate scale called the mesoscopic one.

2. The magnetic phase tensor state variable

2.1. Tensor representation of magnetic structures

The drawings of Figure 1 have been made with the help of experimental observations on various ferromagnetic metals and alloys [4-7] and micro magnetic arguments [6,7]. It is hard to imagine being able to identify this natural heterogeneity with the help of only one macroscopic global measurement, except if we preliminary know the way the structure will establish itself (The use of deterministic methods may moreover permit to limit the number of measurements needed). The dilemma is the same as the one that consists of distinguishing two different subdivisions, that cannot be separated by looking at one macroscopic quantity only. Unfortunately, we clearly feel that if we fix the property of a material previously homogenised, we may predict the response of one sample, but we also might not be able to do it for another geometry [8,9]. Magnetic objects have got typical and characteristic topological and physical properties that we propose to describe thanks to one tensor state variable $[\Lambda^2]$, statistically gathering every microscopic information.

$$[\Lambda^2]=\begin{bmatrix}\Lambda_{11}^2 & \Lambda_{12}^2 & \Lambda_{13}^2\\ \Lambda_{21}^2 & \Lambda_{22}^2 & \Lambda_{23}^2\\ \Lambda_{31}^2 & \Lambda_{32}^2 & \Lambda_{33}^2\end{bmatrix},\begin{Bmatrix}\Lambda_{ii}^2\propto\lambda_j\lambda_k;\ \ j,k\neq i \text{ and } i=1..3\\ \Lambda_{ij}^2\propto\lambda_k^2;\ \ k\neq j\neq i \text{ and } i,j=1..3\end{Bmatrix} \tag{1}$$

Where λ_i, λ_j and λ_k might correspond (with some topological, interaction and averaging corrections) to the typical shape and size of each cell constituting the magnetic structure [2, 10, 11].

$$\lambda_j\ \lambda_k\ \approx\left(2\sigma_e J_s S_{w,jk}\sqrt{n_{w,j}n_{w,k}m_{w,j}m_{w,k}}\right)^{-1}\propto \text{length}^2 \tag{2}$$

σ_e is the electrical conductivity, J_s is the saturation magnetic polarisation, n_w is the walls volume density, m_w is the walls mobility and $S_{w,jk}$ is the walls surface. Each factor of this tensor is homogeneous to a squared length, linked to walls density, surface, mobility, domains size [10,11] … The model is inspired from the Néel domains phase model [6]. The use of (1) is not limited to perfect grain-oriented steels with domains polarization parallel or anti-parallel to the rolling direction ($[\Lambda^2]$ is a diagonal matrix in this case). It is supposed to describe all kinds of magnetic structures in every direction. Of course, using one degree of freedom for three dimensions microscopic objects, we still may not discern different magnetic structures that have got comparable space variations and mesoscopic properties. However, it should have no consequence because it contains a minimum required information concerning the resulting geometry dependent vector behaviour; phenomenon that we aim to consider. Finally, we will need to use the inverse tensor [V] of [Λ] (such that $[V]=[\Lambda]^{-1}$ with $[\Lambda^2]=[\Lambda]^2$ and $[V^2]=[V]^2=[\Lambda]^{-2}=[\Lambda^2]^{-1}$). In the next section, we propose a theory that may provide an alternative to foresee and calculate this mesoscopic diversity.

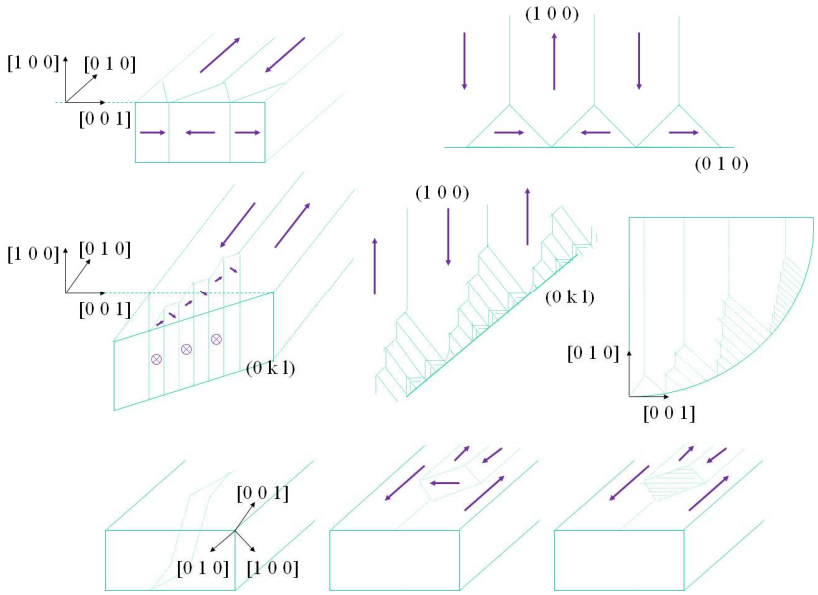

Figure 1: Some heterogeneity and non-uniformity effects. Re-orientation, multiplication and refinement within the microscopic magnetic structure [3-5]. Surface, bulk and non-closure domains examples as a function of the texture, i.e. the crystal axes [m,n,p] and the crystal planes (j,k,l).

2.2. Split Magnetic structure

Microscopic magnetic objects have got typical and characteristic topological and physical properties that we have proposed to describe thanks to one tensor state variable $[\Lambda^2]$, statistically gathering every microscopic information [20]. It is related to mean length of one pair of domains, and so it can be viewed as the sum (3) of two new tensor variables $[\Lambda\uparrow^2]$ and $[\Lambda\downarrow^2]$ in order to account for the actual organisation with opposite neighbouring domains without any loss of generality (*i.e.* including 90° walls and any kind of walls).

$$[\Lambda^2] = [\Lambda_\uparrow{}^2] + [\Lambda_\downarrow{}^2] \tag{3}$$

Equation (3) is similar to a volume conservation law. $[\Lambda^2]$, $[\Lambda\uparrow^2]$ and $[\Lambda\downarrow^2]$ can only be diagonal for magnetic structures containing mainly 180° walls. With 90° walls and other kinds of walls, non-diagonal terms must be considered. Each tensor varies in space and time like $[\Lambda^2]$; They will be our degrees of freedom. We will then define the magnetic polarisation of a soft material with these two tensors and with the natural saturation polarisation (the one carried by each domain of constant magnetisation).

2.3. Magnetic polarization

J_s being the saturation magnetic polarisation, we can define the the local magnetic polarisation $\vec{J}(\vec{x},t)$ by equation (4).

$$[\Lambda^2]\vec{J} = \left([\Lambda_\uparrow{}^2] - [\Lambda_\downarrow{}^2]\right)\vec{J}_s \Leftrightarrow \vec{J} = [V^2]\left([\Lambda_\uparrow{}^2] - [\Lambda_\downarrow{}^2]\right)\vec{J}_s \tag{4}$$

We saw that if the three tensors involved are symmetrical and written with real coefficients [21], they are diagonalisable [15] (see previous paper and definition of $[\Lambda^2]$). We can also show that the basis in which $[\Lambda\uparrow^2]$ and $[\Lambda\downarrow^2]$ are diagonal might be exactly the same and at every point $(\vec{x},t)$, even if it can be different from point to point. This assertion simply comes from the fact that there can exist an anisotropy and identical easy axes for polarisation vectors that are oriented in opposite directions [8]. When (4) is written in the basis B_d that makes all the tensors diagonal, then $\vec{J}_s$ writes $\vec{J}_s=J_s(1,1,1)^T$. Moreover, even if $[\Lambda\uparrow^2]$ and $[\Lambda\downarrow^2]$ vary in space and time with different values for magnetized materials, as for $[\Lambda^2]$ and $\vec{J}_s$ a magnetic state will be defined with $[\Lambda^2]\vec{J} = \left([\Lambda_\uparrow{}^2] - [\Lambda_\downarrow{}^2]\right)\vec{J}_s$ a vector approximately constant in space (with neither divergence nor rotational properties). If we know the temporal and spatial evolutions of tensor $[\Lambda^2]$, then we can easily deduce the magnetic polarisation $\vec{J}$ with the help of (4).

3. Energy contributions at the mesoscopic scale

The natural structuring and its space variations stem from a competition between several energy terms [14]. The contributions proposed are all expressed in $J.m^{-3}$ (volume energy density), except $\vec{e}_{dm}$ which is homogeneous to a surface energy density ($J.m^{-2}$) (the symbols like •, .×, [∇×], $\overrightarrow{\odot}$, and ∴ are explained in the Appendix [15]).

3.1. The mesoscopic magnetic exchange energy

The interaction between neighbouring domains and walls involves an amount of energy $\vec{e}_{ex}$ that we propose to write as follows

$$\vec{e}_{ex} = C_{ex}\frac{\gamma_w^6}{K_{an}^5}\left([\nabla]\times[\Lambda^2]^{-1}\right)\overrightarrow{\odot}^2 \tag{5}$$

γ_w is the walls energy density $[J.m^{-2}]$.

$K_{an}=|\vec{K}_{an}|$ is the module of the macroscopic anisotropy vector $[J.m^{-3}]$.

C_{ex} is a magnetic exchange coefficient without any dimension [n.u.].

This energy vector describes a natural tendency of the material (called *Mesoscopic Exchange Energy*) to make homogeneous its magnetic structure and magnetization. This effect may be even more important when the wall energy is strong ($\gamma_w >> \Lambda K_{an}$) and the anisotropy is weak ($\Lambda K_{an} << \gamma_w$). $[v]=[\nabla]\times[\Lambda^2]^{-1}$ corresponds to a non-divergent magnetic tensor of exchanging walls, that takes part to the energy.

3.2. The mesoscopic magnetic anisotropy energy

This second energy vector $\vec{e}_{an}$ describes another tendency (called *Mesoscopic Anisotropy Energy*) that leads the material to orientate its domains and walls along one or several directions, determined by the most favourable mesoscopic anisotropy axes. The latter, involved in $\vec{K}_{an}$, depend on both the crystallographic texture and metallographic assembly in grains, including the defects [16,17]. This energy depends on the difference between natural and actual directions, weighted by walls equivalent density (Λ^{-2}) and the ratio (γ_w/K_{an}) to take the walls energy, partly due to the microscopic anisotropy, into account. The accurate formulation of this contribution shall depend on the type of anisotropy (uniaxial, bi-axial or tri-axial anisotropy with hexagonal, cubic or more complex symmetry) of the material in use.

$$\vec{e}_{an} = C_{an}\frac{\gamma_w^4}{K_{an}^3}\left([\Lambda^2]^{-1} - \left(\frac{\vec{K}_{an}\cdot\left([\Lambda^2]^{-1}\cdot\vec{K}_{an}\right)^T}{|\vec{K}_{an}|^2}\right)^T\right)^{\overrightarrow{\odot}^2} \tag{6}$$

C_{an} is a macroscopic anisotropy coefficient without any dimension [n.u.].

3.3. The mesoscopic self-magnetostriction energy

This energy vector $\vec{e}_{\lambda\varepsilon}$ describes another tendency (called *Mesoscopic Self Magnetostriction Energy*) that leads to a magnetization induced strain in the material and thus a magneto-elastic energy. The directions of the magneto-strictive strains are determined by the orientations of the polarized domains (each domain carries a magnetic polarization which corresponds to the saturation polarization in a direction given by the domain orientation). We propose equation (7) to describe the fact that the strains magnitude and the corresponding self-magnetostriction energy depend on the magnetostriction coefficients λ_{100} and λ_{111} in directions [100] and [111] respectively [22], the magnetoelastic properties of the material, and the equivalent size Λ of domains.

$$\vec{e}_{\lambda\varepsilon} = +\frac{9}{4}C_\lambda\frac{\gamma_w^4}{K_{an}^4}[\Lambda^2]^{-1}\overrightarrow{\odot}\left([\lambda^2]\therefore[C]\therefore[\Lambda^2]^{-1}\right) \tag{7}$$

[λ] is a magnetostriction tensor with [100] for the diagonal and [111] for the non-diagonal terms. [C] is a stiffness tensor containing the linear elastic properties of an orthotropic or isotropic material [25].

$$[\lambda^2] = \begin{bmatrix} \lambda_{100}^2 & \pm\lambda_{111}^2 & \pm\lambda_{111}^2 \\ \pm\lambda_{111}^2 & \lambda_{100}^2 & \pm\lambda_{111}^2 \\ \pm\lambda_{111}^2 & \pm\lambda_{111}^2 & \lambda_{100}^2 \end{bmatrix} \text{ and } [C] = \begin{bmatrix} C11 - C12 & C44 & C55 \\ C44 & C22 - C23 & C66 \\ C55 & C66 & C33 - C13 \end{bmatrix} \quad (8)$$

C_λ is a magnetostriction coefficient without any dimension.

3.4. The mesoscopic magneto-strictive stress induced anisotropy energy

This energy vector $\vec{e}_{\lambda\sigma}$ (called *Stress Induced Anisotropy Energy*) describes the change in anisotropy and in the magnetization due to an external stress. The directions of the stresses define the new directions to be considered in the total macroscopic anisotropy [22, 25]. We propose equation (9) to describe the fact that the stress induced energy depends on the magnetostriction coefficients λ_{100} and λ_{111}, the stress value and the equivalent size Λ of domains in each stress direction.

$$\vec{e}_{\lambda\sigma} = -\frac{3}{2} C_\lambda \frac{\gamma_w^4}{K_{an}^4} [\Lambda^2]^{-1} \overrightarrow{\odot} \left([\lambda] \div [\sigma] \div [\Lambda^2]^{-1} \right) \quad (9)$$

[σ] is the stress tensor [Pa].

3.5. Mesoscopic energy loss due to microscopic eddy currents

Any physical mechanism that leads to a new magnetic structure costs some energy $\vec{e}_\tau$. We know that any change in the magnetic structure is not reversible, but rather dissipative with losses. The latter mainly come from eddy currents induced around the walls in motion and in magnetic domains with rotating magnetization. Let's assume that any change in the global magnetic energy minimum, which is responsible for the change in magnetization and magnetic structure, can only increase in time due to eddy current losses induced by the time variations of $[\Lambda^2]$.

$$\vec{e}_\tau = +\frac{\gamma_w^4}{K_{an}^3} \tau \partial_t [\Lambda^2]^{-1} \overrightarrow{\odot} [\Lambda^2]^{-1} \quad (10)$$

τ [ms] is a time delay related to the magnetic field damping, which is due to microscopic eddy currents induced around moving walls and inside magnetic domains where the magnetization rotates. This effect can be considered as a damper equivalent to a dynamic induced anisotropy always perpendicular to the directions given by $[\Lambda^2]$.

3.6. The mesoscopic dipolar demagnetizing energy

Finally, the last energy term is mainly due to the surface dipolar magnetic energy related to magnetic poles.

$\vec{n}$ being the unit vector normal to the outer surface of the geometry considered. C_{dm} is a metallurgical parameter that can depend on the grain's boundary spacing and any surface treatment (surface laser treatment with a lines' depth and spacing for example)

$$\vec{e}_{dm} = C_{dm} \frac{K_{an}^4}{\gamma_w^3} \left(\vec{n} \cdot \left([\Lambda^2] \cdot \vec{n} \right)^T \right) \overrightarrow{\odot 2} \quad (11)$$

This vector tends to orientate the magnetic moments [5], multiply and refine the domains, in order to create as few and distant poles as possible. The energy vector $\vec{e}_{dm}$ is different from zero on the surface only (the material often manages to create a minimum charge within the bulk, even if it cannot avoid it onto the surface) [12,13]. This energy is even more important that the surface domains are big, the anisotropy is strong, and the walls energy is weak. In one of the next sections and in the next deliverable update, we will propose to develop a surface and coupling model to describe the surface magnetic structure, minimizing the energy terms that correspond to this surface. C_{dm} is one of the key parameters that determines Λ at the surface.

4. Energy driven tensor magnetic structuration

4.1. Total energy minimization principle

The magnetic structure will establish itself by minimising the total following energy of the system {volume Ω, outer surface ∂Ω}

$$\vec{E}_m = \iiint_\Omega (\vec{e}_m) d^3x = \iiint_\Omega (\vec{e}_{ex} + \vec{e}_{an} + \vec{e}_{\lambda\epsilon} + \vec{e}_{\lambda\sigma} + \vec{e}_\tau) d^3x$$
$$+ \iint_{\partial\Omega} (\vec{e}_m + \vec{e}_{dm}) d^2x \quad \text{to be lowered} \quad (12)$$

This description can be developed thanks to additional contributions due to miscellaneous parameters: volume charges, temperature, surface texture, surface or/and volume induced stress… Finally, each contribution appears here quasi-static without any field interactions. The coupling with the quasi-static magnetic field can be considered with a border static condition. The dynamic diffusion and the coupling with the time varying field may be considered afterwards with the Maxwell Equations [2,10], or with the volume dynamic term $\vec{e}_\tau$ and with a border's dynamic condition (see [11] and [21]).

4.2. Physical non divergence assumptions

We study first the ensemble {Exchange, Anisotropy} weakly varying the tensor $[\Lambda^2]$ (see Appendix for usual identities). We assume that the material has succeeded in minimising its magnetic charges, by orientating most of its domains and walls tangentially to the surface, or by

multiplying and refining them. So, we also have

$$\iint_{\partial\Omega}\left[\Lambda^2\right]\cdot\vec{n}\,d^2x=\iiint_{\Omega}\vec{\nabla}\cdot\left[\Lambda^2\right]d^3x=\vec{0}\Leftrightarrow\vec{\nabla}\cdot\left[\Lambda^2\right]=\vec{0} \tag{13}$$

The divergence of $\vec{J}$ is closely linked to the one of $[\Lambda^2]$ (14) ($\left[\vec{\nabla}\otimes\vec{J}_s\right]=[0]$, explanations given in the Appendix)

$$\vec{\nabla}\cdot\vec{J}=\vec{\nabla}\cdot\left([V^2]\left([\Lambda_\uparrow{}^2]-[\Lambda_\downarrow{}^2]\right)\right)\vec{J}_s \tag{14}$$

The non-divergence condition on $[\Lambda^2]$ is so closely linked to the one acting on $\vec{J}$. In fact, we have the obvious and certain following implication (with (3) and $\vec{\nabla}.\vec{J}=0$, we can show that the reciprocal relation of (15) is also true)

$$\begin{aligned}\vec{\nabla}\cdot\left([V^2][\Lambda_\uparrow{}^2]\right)=\vec{\nabla}\cdot\left([V^2][\Lambda_\downarrow{}^2]\right)=0\\ \Leftrightarrow\vec{\nabla}\cdot\vec{J}=0\end{aligned} \tag{15}$$

The variational principle applied onto the action E_m seems to give us two interesting clues [18].

4.3. Borders and physical boundary conditions

First the matrix $[n]\otimes\left([\nabla]\times[\Lambda^2]^{-1}\right)$ keeps constant at each interface of $\partial\Omega$ surrounding any volume Ω. It does not exist in substances without any domains and walls; it will therefore be nil at the edge between such a classical material and a structured one. It means that the rotational evolutions within the magnetic structure stop against the outer surface along its normal unit vector.

It seems that the non-divergence condition on $[\Lambda\uparrow^2]$ and $[\Lambda\downarrow^2]$ implies the absence of volume charges because then $\vec{\nabla}\cdot\vec{J}=0$ (15). However there can always exist surface charges depending on the direction of $\vec{J}$ and polarisations of surface domains relative to the normal vector of the enclosing surface, even if the divergence theorem [8] tells us that the global surface integrals $\oiint_{\partial\Omega}([\Lambda^2]\cdot[n])d^2x$ and $\oiint_{\partial\Omega}(\vec{J}\cdot\vec{n})d^2x$ equal thus 0 [20].

4.4. Partial differential tensor equation

Secondly, the tensor property into any volume Ω obeys the following partial differential equation:

$$\begin{aligned}&[\Delta]\ [V^2]-\vec{\nabla}\left(\vec{\nabla}.[V^2]\right)-\frac{C_{an}}{C_{ex}}\left(\frac{K_{an}}{\gamma_w}\right)^2\left([V^2]-\left(\frac{\vec{K}_{an}([V^2]\vec{K}_{an})^T}{K_{an}^2}\right)^T\right)\\ &+\frac{3}{2}\frac{C_\lambda}{C_{ex}}\left(\frac{K_{an}}{\gamma_w}\right)^2\left(\frac{[\lambda]\therefore[\sigma]}{K_{an}}\therefore[V^2]\right)-\frac{9}{4}\frac{C_\lambda}{C_{ex}}\left(\frac{K_{an}}{\gamma_w}\right)^2\left(\frac{[\lambda^2]\therefore[C]}{K_{an}}\therefore[V^2]\right)-\left(\frac{K_{an}}{\gamma_w}\right)^2\tau\partial_t[V^2]=[0]\end{aligned} \tag{16}$$

We call this equation the tensor structuring equation for the magnetic structure.

We define κ [mm^{-2}] the squared ratio between the total anisotropy (either magneto-crystalline, magneto-strictive or stress induced) and the magnetic exchange:

$\kappa = \kappa_{an} + \kappa_{\lambda\varepsilon} - \kappa_{\lambda\sigma}$

$=(C_{an}/C_{ex})*(K_{an}/\gamma_w)^2 + (C_\lambda/C_{ex})*(K_{an}/\gamma_w)^2(9\lambda^2C/4K_{an}) - (C_\lambda/C_{ex})*(K_{an}/\gamma_w)^2(3\lambda\sigma/2K_{an})$

κ determines both the preferred components of $[V^2]=[\Lambda^2]^{-1}$ and its space variations in the mass (structuring depth).

$\kappa_{\lambda\varepsilon}$ is always positive and corresponds to an equivalent negative compressive stress.

$\kappa_{\lambda\sigma}$ can contain the manufacturing residual stress (rolling and coating processes) or/and induced stress (surface laser treatments). When $\lambda_{100} > 0$ (positive magnetostriction), $\kappa_{\lambda\sigma}$ is positive for negative compressive stress and negative for positive tensile stress.

Let's define $\kappa_s = \kappa_{\lambda\varepsilon} - \kappa_{\lambda\sigma_r}$ the natural magnetostriction anisotropy due to either self-magnetostriction and manufacturing stress (σ_r being the global residual stress) and $\kappa_{si} = - \kappa_{\lambda\sigma i}$ the surface induced stress anisotropy ($\sigma_i = \sigma_T$ or σ_m any local surface induced stress).

4.5. Discussions

The worry with this deterministic equation is its matrix nature with lots of unknown variables (maximum 9). Fortunately, and as already mentioned [11], $[\Lambda^2]$ and $[V^2]$ will probably be real and symmetrical and so diagonalisable, which reduces to 6 or 3 the number of unknown factors [19]. Nevertheless, its implementation is not quite different from a classical diffusion equation; we just have to solve three of them simultaneously. Finally, one initial computation might be enough in most cases. Concerning the determinism, we must say that this formalism can only be used with macroscopic bodies for which a homogenised property has got a significant meaning (global size >> microscopic magnetic objects dimension). We thus do not calculate the exact structure but only its spatial and statistical average and especially its mixed properties related to "mobility", "characteristic dimensions", "preferred directions" … It is moreover possible to imagine manipulating several powers of tensor [V] in the structuring phenomenon, to be faithful to actual and natural microscopic multiple and series-like organisations. This description may be profitable in theoretical exploring for structured soft materials in terms of loss and behavioural consequences; attractive for computer-aided design and accurate simulations purposes. Providing a coupled model to describe the surface magnetic structure sensitive to the grain boundaries, texture and surface laser treatments, it might be possible to help the specification of some aspects of manufacturing processes (laser parameters and patterns for example).

5. Surface magnetic field coupling and observables

When a varying magnetic field is applied to the material, some memory effects (called hysteresis) and eddy currents are induced within the microscopic mechanisms around defects and magnetic walls and inside magnetic domains. It manifests itself in a magnetic behaviour, characterised by a delayed relationship between the magnetic field $\vec{H}$ and the flux density or induction $\vec{B}$.

5.1. Vector magnetic behaviour

5.1.1. The quasi-static an-hysteretic field $\vec{H}_M$

The quasi-static an-hysteretic field $\vec{H}_M$ corresponds to an equilibrium for the magnetic structure, the one that would induce neither any hysteresis nor losses. This equilibrium is usually described with the following magnetic law:

$$\vec{H}_M(\vec{B}) = \nu\vec{B} = \mu^{-1}\vec{B} \tag{17}$$

$\mu=\nu^{-1}$ and ν are the quasi-static magnetic permeability and reluctivity respectively [H/m]. They can be scalar or tensor, linear or not.

5.1.2. Static hysteretic field $\vec{H}_s$

The static hysteresis is mainly due to hampering and jumps of magnetic walls [24] around defects, grains joints… and local microscopic unavoidable magnetic charges. Changes in the applied magnetic field can make the walls move when a threshold is excited to counterbalance the opposition of the charges. Then the walls irreversibly jump, inducing eddy currents and losses. It naturally usually depends on the history of the material (existing structure and hampered walls on defects plus succession of field applied [11]). Considering our purpose which is mainly to model the magnetic structure and the frequency dependent vector behaviour and losses, we decide not to add more difficulties to this study by assuming that $\vec{H}_s$ corresponds approximately to the coercive loss field which depends on $\vec{B}$:

$$\vec{H}_s(\vec{B}) \approx \underline{\nu}_c\vec{B} = j\nu_c\vec{B} \tag{18}$$

$\underline{\nu}_c = j\nu_c$ is the complex coercive reluctivity (static hysteresis field that gives the hysteresis loss other the flux density) [m/H]. However, the present description can be implemented by starting with a particular and unic initial condition for the magnetic domains (related to the past history), i.e. a distribution in space.

5.1.3. Dynamic hysteretic field $\vec{H}_{dyn}$

The dynamic hysteresis is mainly due to eddy currents induced with time varying fields and polarisations at the mesoscopic scale within domains and at the microscopic scale around moving domain walls [26]. They can be homogenised and included in a behavioural model, dedicated to the magnetic field damping and involving the tensor variable $[\Lambda^2]$.

$$\vec{H}_{dyn}(\vec{B}, \partial_t\vec{B}) = \sigma_e[\Lambda^2](\vec{B}, \partial_t\vec{B})\,\partial_t\vec{B} \tag{19}$$

σ_e is the electrical conductivity [S/m].

5.1.4. Total magnetic field

All these phenomena "delay" the flux density or the induction $\vec{B} = \mu_0\vec{H}+\vec{J} = \mu_0(\vec{H}+\vec{M})$ such that the magnetic field $\vec{H}$ (20) becomes the sum of the quasi-static magnetic field $\vec{H}_M$ ([11], the excess static hysteresis field $\vec{H}_s(\vec{B})$ due to hysteresis and the dynamic field $\vec{H}_{dyn}(\vec{B}, \partial_t\vec{B})$ due to motion of domain walls (see Figure 2 and (20)) ($\mu_0=4\pi.10^{-7}$ H/m is the vacuum magnetic permeability.)

$$\vec{H}(\vec{B}, \text{History}, \partial_t\vec{B}) = \vec{H}_M(\vec{B}) + \vec{H}_s(\vec{B}, \text{History}) + \vec{H}_{dyn}(\vec{B}, \partial_t\vec{B}) \tag{20}$$

Neglecting the static hysteresis ($\nu_c\mu \ll 1$), the dynamic relationship between the field $\vec{H}$ and the magnetic polarization $\vec{J}$ becomes:

$$\left((1-\nu\mu_0) - \sigma_e[\Lambda^2]\mu_0\,\partial_t\right)\vec{H} = \nu(1+\sigma_e[\Lambda^2]\mu\,\partial_t)\vec{J} \tag{21}$$

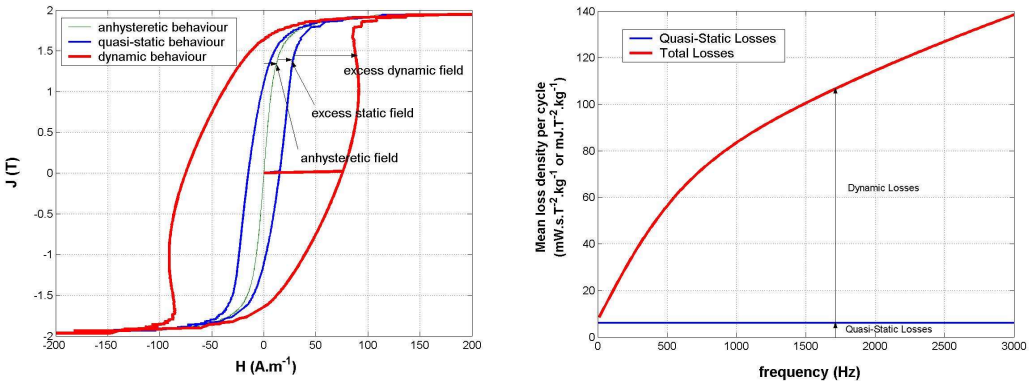

Figure 2: An-hysteretic curve, Static and Dynamic hysteresis (left) / Static and Dynamic Losses (right).

5.2. Surface magnetic field coupling and polarization

Coupling the volume structuring model and the magnetic field consists in using the behavioral law (21) at the surface of the material, involving the surface magnetic structure $[\Lambda_0^2]=[\Lambda^2]_{surf}$, which represents the boundary condition of the model. We suggest analysing the magnetic behaviour with the help of Bode diagrams (see Figure 9). We assume that $[V_0^2]$ is known (next sections for examples) and that

$[\Lambda^2]\vec{J}=[\Lambda_0^2]\vec{J}_{surf}$ is a constant vector, independent from z, that we can determine using (21) at the surface for time harmonics with angle velocity ω ($\vec{H}_a = \vec{H}_{surf}$, $\vec{H}_s = 0$ neglected, $\mu=\mu_0\mu_r=\mu_0(1+\chi)$).

$$\vec{J} = [V^2]\left[\Lambda_0^2\right]\frac{\left[\left(\frac{\chi}{1+\chi}-\nu_c\mu\right)-j\sigma_e\left[\Lambda_0^2\right]\mu_0\omega\right]}{\left[\left(1+\nu_c\mu\right)+j\sigma_e\left[\Lambda_0^2\right]\mu\omega\right]}\mu\vec{H}_a \xrightarrow[\mu_0\ll\mu]{\nu_c\mu\ll 1} \vec{J} \approx [V^2]\left[\Lambda_0^2\right]\left[1+j\sigma_e\left[\Lambda_0^2\right]\mu\omega\right]^{-1}\mu\vec{H}_a \quad (22)$$

Whatever the experimental tool used, we can *a priori* only measure and access the magnetic field $\vec{H}_a$ applied onto the enclosing surface and the mean flux density $<\vec{B}>_r$, averaged inside the volume Ω considered. In some usual and convenient configurations (closed magnetic circuit), the mean magnetic polarisation $<\vec{J}>_r$ can also be determined. $\vec{J}$ checks (22) and $\vec{H}$ can be given by (21). It is finally possible to build the magnetic behaviour $<\vec{B}>_r(\vec{H}_a)$ and the averaged total loss density $<<p>_r>_t=<\vec{H}_a<\partial_t\vec{B}>_r>_t$.

5.3. Definition of macroscopic observables

5.3.1. The apparent magnetic permeability

To study the magnetic response, we examine the reduced apparent permeability defined in our case by (23):

$$\frac{\vec{\mu}_{app}}{\mu} = \frac{\langle\vec{J}\rangle_r}{\mu H_a} = \frac{1}{\zeta}\int_{-\zeta/2}^{+\zeta/2}\frac{\vec{J}}{\mu H_a}dz \quad (23)$$

5.3.2. The total magnetic losses

The mean total power loss density becomes the sum of two contributions:

$$\begin{aligned}\ll p >_r>_t &=< \vec{H}_{surf} < \partial_t\vec{J} >_r>_t =\ll p_{stat} >_r>_t + \ll p_{dyn} >_r>_t \\ &=< \vec{H}_{s,surf} < \partial_t\vec{J} >_r>_t + < \vec{H}_{dyn,surf} < \partial_t\vec{J} >_r>_t \end{aligned} \quad (24)$$

The fields acting are applied onto the enclosing surface. $<.>_r$ means a volume average in space and $<.>_t$ means a time average operation. No classical losses appear here. All the contributions due to varying induced "diffusion" are supposed to be included in the dynamic term (see (16), (20) and Figure 2), where $\vec{H}_{dyn,surf}$ and $<\partial_t\vec{J}>_r$ contain every damping effect due to heterogeneous and non-uniform domain walls motion and eddy currents as well.

6. 1D static and magneto-harmonic test case and sensitivity analysis

We propose here to apply the previous method onto one simple geometry (1D steel sheet of width ζ, Figure 3) with two materials of different anisotropies (§ 6.1.1.: perfectly oriented steel with texture parallel to the lamination plan and with one easy x direction, § 6.1.2.: partially oriented steel with texture parallel to the lamination plan and with 2 possible favourable axes, x or y)

$$\begin{aligned}&\partial_z^2[V^2] - \frac{C_{an}}{C_{ex}}\left(\frac{K_{an}}{\gamma_w}\right)^2\left([V^2] - \left(\frac{\vec{K}_{an}([V^2]\vec{K}_{an})^T}{K_{an}^2}\right)^T\right) \\ &+\frac{3}{2}\frac{C_\lambda}{C_{ex}}\left(\frac{K_{an}}{\gamma_w}\right)^2\left(\frac{[\lambda]\cdot\cdot[\sigma]}{K_{an}}\cdot\cdot[V^2]\right) - \frac{9}{4}\frac{C_\lambda}{C_{ex}}\left(\frac{K_{an}}{\gamma_w}\right)^2\left(\frac{[\lambda^2]\cdot\cdot[C]}{K_{an}}\cdot\cdot[V^2]\right) - j\left(\frac{K_{an}}{\gamma_w}\right)^2\tau\omega[V^2]=[0]\end{aligned} \quad (25)$$

Let's consider a magnetic sheet of thickness ζ. Let's use the (x,y,z) or (1,2,3) reference frame for which axis 1 or x corresponds to the rolling direction, 2 or y corresponds to the transverse direction and z corresponds to the thickness (see Figure 3). The 1D approximation consists in assuming no space variation in directions x and y but only in direction z. We also consider only time harmonics variations. The Partial Differential Equation PDE (16) becomes (25). Let's work with a perfectly (GO) or partially (GO) oriented material of mass density d, linear properties (magnetic permeability $\mu=\nu^{-1}=\mu_r\mu_0$ and electric conductivity $\sigma_e=\rho^{-1}$). We will focus onto the average magnetic polarisation and the mean power losses within time harmonics (frequency f and $\omega=2\pi f$). We will highlight the role played by both the geometry and the magnetic structure on these global quantities.

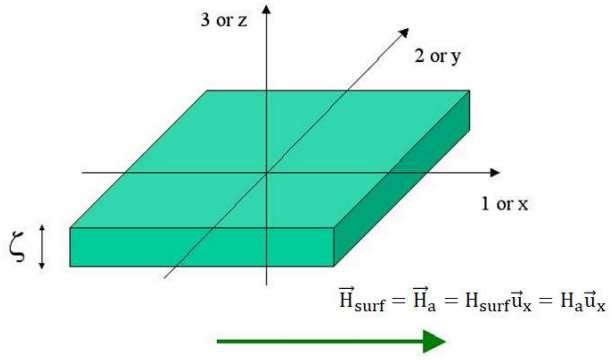

Figure 3: Geometry of the 1D test case studied

6.1. Calculation of magnetic structures

6.1.1. Grain Oriented electrical steel

For perfectly grain oriented materials, we assume that the anisotropy vector $\vec{u}_{an}$ can be written as follows in the (x,y,z) basis:

$\vec{u}_{an}=\vec{K}_{an}/K_{an}=(1,0,0)^T$. We are looking for the tensor $[V^2]=[V^2_{ij}]$, that obeys equation (25), knowing the boundary conditions acting on its components $V^2_{ii0}=V^2_{ii}(z=\pm\zeta/2)$, (i=1,2,3). The magnetic structure can be approximately described with a diagonal tensor $[V^2]=[\Lambda^2]^{-1}$:

$$[V^2]=\begin{bmatrix} V_{11}^2 & 0 & 0 \\ 0 & V_{22}^2 & 0 \\ 0 & 0 & V_{33}^2 \end{bmatrix} \tag{26}$$

We use the following input parameters and boundary conditions:

ζ=0.5 mm and $\kappa_{an}=\frac{C_{an}}{C_{ex}}\left(\frac{K_{an}}{\gamma_w}\right)^2=(4/\zeta)^2$ mm^{-2} with $\vec{u}_{an}=(1,0,0)^T$.

Λ_{110} = 100 µm, $\Lambda_{220}=\Lambda_{330}$ = 200 µm, $\Lambda_{120}=\Lambda_{130}=\Lambda_{230}=10^4$ µm >> at the surface.

The PDE corresponding to the three unknowns V^2_{ii} (i=1..3) are:

$$\left(\partial_z^2.-\kappa_{ii}(1+\tau_{ii}\,\partial_t.)\right)V^2_{ii}=0 \tag{27}$$

With

$\kappa_{11}=\kappa_{S,11}$ and $\kappa_{ii}=\kappa_{an}+\kappa_{s,ii}$ for i=2,3

$$\kappa_{s,ii}=\frac{C_\lambda}{C_{ex}}\left(\frac{K_{an}}{\gamma_w}\right)^2\left(\frac{3\lambda_{100}}{2K_{an}}\right)\left(\frac{3}{2}\lambda_{100}-\sigma_{ii}\right),\sigma_{ij}=0$$

$$\tau_{ii}=\left(\frac{K_{an}}{\gamma_w}\right)^2\tau\Big/\kappa_{ii}$$

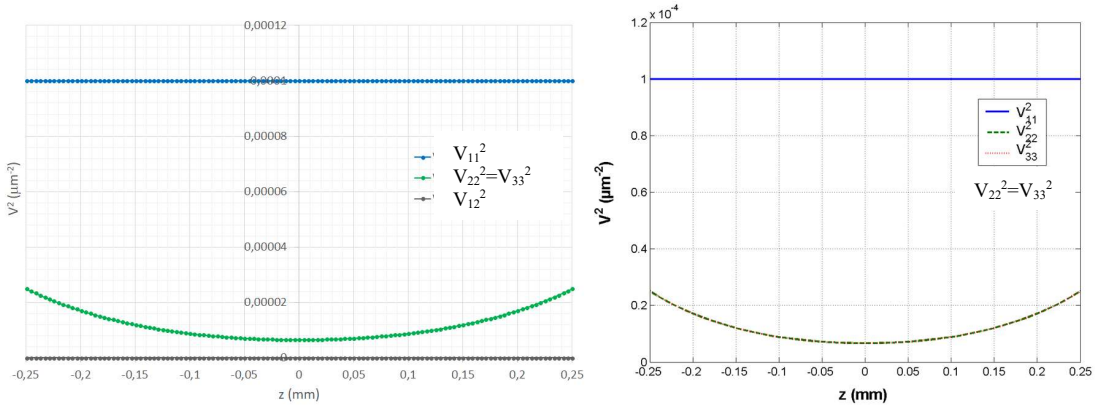

Figure 4: Calculation of the tensor $[V^2]$ in GO steels with the Finite Element Method (left) and analytical formulae given above (right) with κ_s=0 and τ=0.

The time harmonic solutions with angle velocity ω are given by:

$$V^2_{ii}(z)=V^2_{ii0}\frac{\cosh\left(\sqrt{\kappa_{ii}(1+j\tau_{ii}\omega)}z\right)}{\cosh\left(\frac{\sqrt{\kappa_{ii}(1+j\tau_{ii}\omega)}\zeta}{2}\right)},\quad i=1,2,3 \tag{28}$$

The model can be implemented either with analytical formulae (linear 1D testcases only) or the finite element method (useful for larger dimensions). Results are shown in Figure 4. Looking at the results, we notice as expected, that the highest contribution to the tensor $[V^2]$ (and consequently to $\vec{J}$), which is constant in steel thickness, might be the first component parallel to the easy direction. But there may be other small varying contributions perpendicular to the easy direction because of unavoidable reorganisations, exchanges and surface effects in the magnetic structure. The consequences are even more significant when the material is not perfectly oriented, when the field is disorientated or when the geometry is thick (see next §).

6.1.2. Non-Grain oriented electrical steel

For non-grain oriented materials, we work with the anisotropy vector $\vec{u}_{an}=\vec{K}_{an}/K_{an}=(a,b,0)^T$ ($a^2+b^2=1$, we find the previous case again with a=1 and b=0). We are looking for $[V^2]=[V^2_{ij}]$, that obeys equation (25), knowing the boundary conditions acting on its components $V^2_{ij0}=V^2_{ij}(z=\pm\zeta/2)$, (i,j=1,2,3). The magnetic structure can be approximately described with a non-diagonal tensor $[V^2]=[\Lambda^2]^{-1}$.

$$[V^2]=\begin{bmatrix} V_{11}^2 & V_{12}^2 & 0 \\ V_{21}^2 & V_{22}^2 & 0 \\ 0 & 0 & V_{33}^2 \end{bmatrix} \tag{29}$$

We use the following input parameters and boundary conditions:

ζ=0.5 mm and $\kappa_{an}=\frac{C_{an}}{C_{ex}}\left(\frac{K_{an}}{\gamma_w}\right)^2=(4/\zeta)$ mm^{-2} with $\vec{u}_{an}=(a=\sqrt{(2/3)},b=\sqrt{(1/3)},0)^T$.

$V^2_{120} = V^2_{210} = -(0.75/300)^2$, $V^2_{130} = V^2_{230} = -(1/10000)^2$, $V^2_{110} = (2/300)^2$, $V^2_{220} = (1/300)^2$, $V^2_{330} = (0.5/300)^2$ µm^{-2} at the surface.

The PDE corresponding to the four unknowns V^2_{ii} and V^2_{12} are:

$$\begin{Bmatrix} \left(\partial^2_z . - \kappa_{ii}(1+\tau_{ii}\,\partial_t .)\right)V^2_{ii} + \kappa_{an} ab V^2_{ij} \\ \left(\partial^2_z . - \kappa_{ij}(1+\tau_{ij}\,\partial_t .)\right)V^2_{ij} - \kappa_{an} ab V^2_{ii} \end{Bmatrix} = \begin{Bmatrix} 0 \\ 0 \end{Bmatrix} \quad (30)$$

We use the following notations

$\kappa_{11} = \kappa_{an}(1-a^2) + \kappa_{s,11}$

$\kappa_{22} = \kappa_{an}(1-b^2) + \kappa_{s,22}$

$\kappa_{33} = \kappa_{an} + \kappa_{s,11}$

$\kappa_{12} = \kappa_{an}(2-b^2-a^2)$

$$\kappa_{s,ii} = \frac{C_\lambda}{C_{ex}}\left(\frac{K_{an}}{\gamma_w}\right)^2\left(\frac{3\lambda_{100}}{2K_{an}}\right)\left(\frac{3}{2}\lambda_{100} - \sigma_{ii}\right), \sigma_{ij} = 0$$

$$\tau_{ij} = \left(\frac{K_{an}}{\gamma_w}\right)\tau \Big/ \kappa_{ij}$$

The time harmonic solutions with angle velocity ω are shown in Figure 5. Looking at this second result, we see that couplings with, and z dependences in, all the components of $[V^2]$ can exist. It is still due to arrangements and exchanges taking anisotropies and surface effects into account. Therefore, it will somehow template the global static and dynamic magnetic properties.

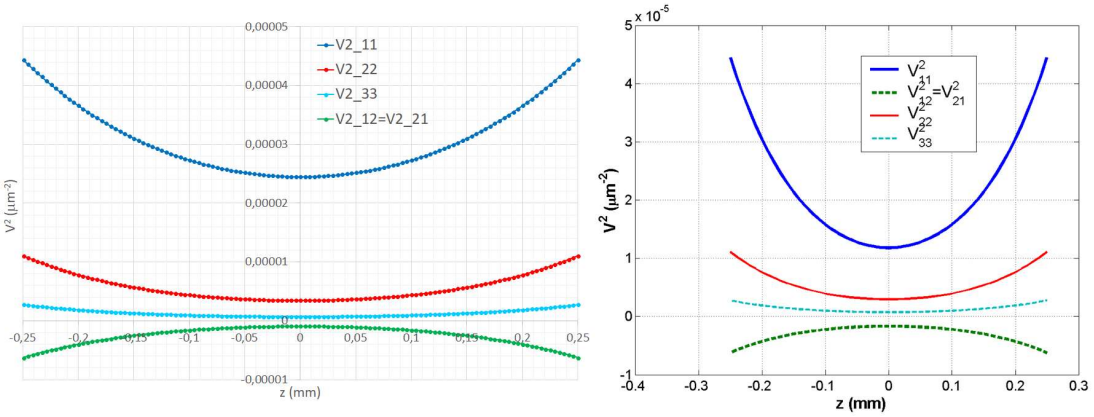

Figure 5: Calculation of the tensor $[V^2]$ in NGO steels with the Finite Element Method (left) and analytical formulae given above (right) with κ_s=0 and τ=0.

6.1.3. Sensitivity analysis – case of GO SiFe

The Figure 6 shows the results of a sensitivity analysis to the main physical parameters κ_{an} (macroscopic magneto-crystalline anisotropy), κ_s (stress induced anisotropy), $\Lambda_0 = \Lambda_{surf}$ (surface magnetic structure) and τ (eddy current or field damping time delay).

The default values of the input parameters used are as follow:

ζ = 0.23 – 0.5 mm (sheet thickness)

J_s = 2.1 T (saturated magnetic polarization)

$\rho = \sigma_e^{-1}$ = 48 µΩ.cm (electrical resistivity)

μ = 20 000μ_0 (quasi-static permeability)

d = 7650 kg.m^{-3} (volume mass density)

κ_{an} = 10-100 mm^{-2} (macroscopic magneto-crystalline anisotropy coefficient, $\vec{u}_{an}=(1,0,0)^T$)

$\kappa_s = \kappa_{s,11} = \kappa_{s,22} = \kappa_{s,33}$ =-100…+100 mm^{-2} (stress induced anisotropy)

τ = 1…60 ms (eddy current damping time delay)

ω = 2*pi*300 (time harmonic angle velocity)

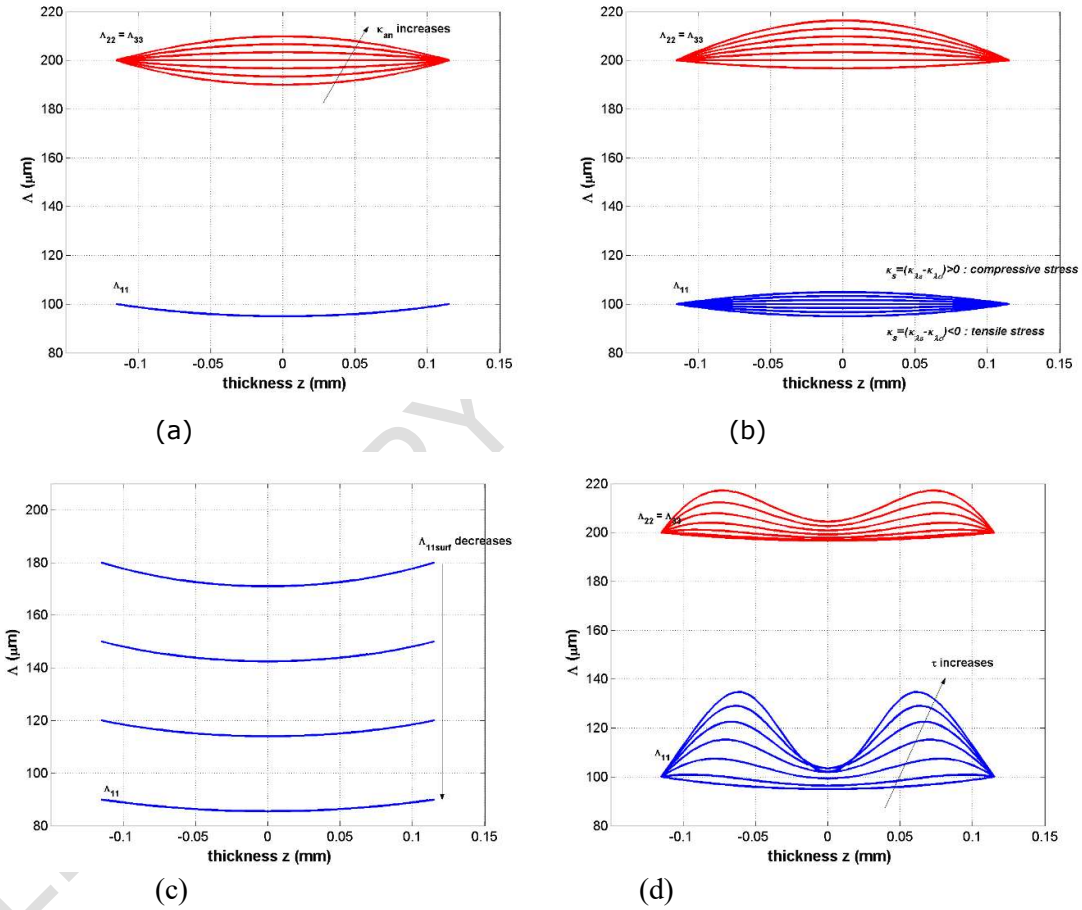

Figure 6: Sensitivity analysis of the GO magnetic structure to the macroscopic magneto-crystalline anisotropy (a), the stress induced anisotropy (b), the surface magnetic structure (c) and the eddy currents time delay (d).

6.2. Calculation and sensitivity analysis of observables – ***case of a perfectly GO material***

6.2.1. Macroscopic vector quasi-static Behaviour

6.2.1.1. Stress induced anisotropy and apparent permeability

By using (22) with $\omega = 0$, $\mu >> \mu_0$ and $\vec{B} \approx \vec{J}$, (23) becomes

$$\frac{\vec{\mu}_{app}}{\mu} = \frac{1}{\zeta}\left(\int_{-\frac{\zeta}{2}}^{+\frac{\zeta}{2}} [V^2]dz\right)[\Lambda_0^2]\frac{\vec{H}_a}{H_a}$$

$$\mu_{app,i} = \frac{\tanh\left(\frac{\sqrt{\kappa_{ii}}\zeta}{2}\right)}{\left(\frac{\sqrt{\kappa_{ii}}\zeta}{2}\right)}\mu \qquad (31)$$

$\vec{H}_a/H_a$ gives the direction of the magnetic field applied on the surface. In this model μ is a scalar, the anisotropy is determined by the magnetic structure, the shape and orientation of magnetic domains and so the tensor $[\Lambda^2]$. However, it is possible to take into consideration non-linearities and additional microscopic anisotropy within a tensor $[\mu]$.

Due to a positive magnetostriction ($\lambda_{100}>0$), Figure 7 shows that a global tensile stress σ_{ii} increases the quasi-static apparent permeability in direction "i" and that a compressive stress σ_{jj} decreases quasi-static apparent permeability in the direction "j".

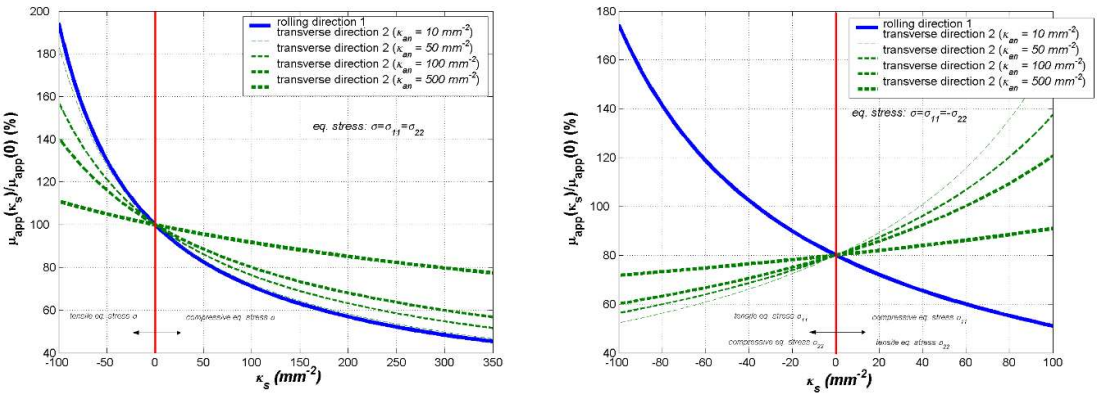

(a) (b)

Figure 7: Sensitivity analysis of static apparent permeability to the magneto-crystalline κ_{an} and stress induced κ_s anisotropies ((a) $\sigma_{11} = \sigma_{22}$ (b) $\sigma_{11} = -\sigma_{22}$).

6.2.1.2. Coercive force and static hysteresis losses

The general definition of the mean power loss density for any periodic signal is given by (24). For time harmonics, the corresponding quasi-static energy loss $\langle\langle\xi_{stat}\rangle_r\rangle_t$ per cycle and per Tesla^2 becomes then (in W.s.T^{-2}.kg^{-1} or J. T^{-2}.kg^{-1})

$$\ll \xi >_r>_t = \frac{\pi \ll p >_r>_t}{d\omega\left|<\vec{J}>_r\right|^2} = \ll \xi_{stat} >_r>_t + \ll \xi_{dyn} >_r>_t$$

$$\xi_s = \ll \xi_{stat} >_r>_t = \mathrm{Re}\left(-j\frac{\pi\vec{\underline{H}}_{s,surf} < \vec{\underline{J}} >_r^*}{d\left|<\vec{\underline{J}}>_r\right|^2}\right) = \sum_i \xi_{si}$$

$$\xi_{si} = \frac{\pi}{d}\mathrm{real}\left(-j\underline{\nu}_c\frac{\tanh\left(\frac{\sqrt{\underline{\kappa}_{ii}}\zeta}{2}\right)}{\left(\frac{\sqrt{\underline{\kappa}_{ii}}\zeta}{2}\right)}\right) \quad (32)$$

The relative variation of quasi-static losses as a function of the anisotropies are the same as the ones for the quasi-static apparent permeability given in Figure 7. Due to a positive magnetostriction ($\lambda_{100}>0$), a global tensile stress σ_{ii} increases the quasi-static losses in direction "i" and a compressive stress σ_{jj} decreases quasi-static losses in the direction "j". Therefore, except if the coercive reluctivity depends on the stress, a tensile stress cannot reduce the quasi static losses but rather the dynamic losses (see Figure 10).
Figure 8 gives results of the sensitivity analysis to the coercive reluctivity. The quasi-static losses are proportional to ν_c, but the slope depends on the anisotropies and especially on the stress induced anisotropy.

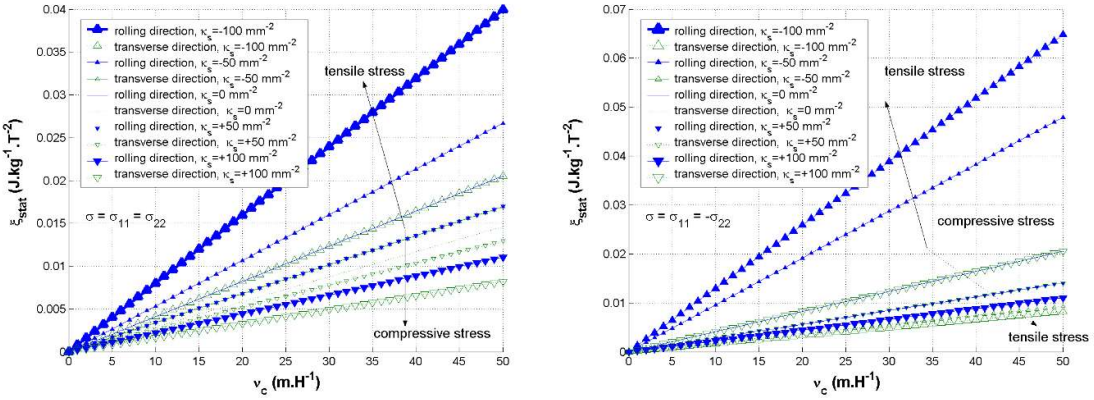

(a) (b)

Figure 8: Sensitivity analysis of static losses to the coercive reluctivity ν_c and the stress induced κ_s anisotropy with κ_{an} = 100 ((a) $\sigma_{11} = \sigma_{22}$ (b) $\sigma_{11} = -\sigma_{22}$).

6.2.2. Macroscopic vector dynamic Behaviour
6.2.2.1. Frequency dependent apparent permeability

By using (22) with $\omega \neq 0$, $\mu >> \mu_0$ and $\vec{B} \approx \vec{J}$, (23) becomes

$$\frac{\vec{\mu}_{app}}{\mu} = \frac{1}{\zeta}\left(\int_{-\frac{\zeta}{2}}^{+\frac{\zeta}{2}}[V^2]dz\right)\left[\Lambda_0^2\right]\left[[1] + j\sigma_e\left[\Lambda_0^2\right]\mu\omega\right]^{-1}\frac{\vec{H}_a}{H_a}$$

$$\mu_{app,i} = \left(\frac{\tanh\left(\frac{\sqrt{\kappa_{ii}(1+j\tau_{ii}\omega)}\zeta}{2}\right)}{\left(\frac{\sqrt{\kappa_{ii}(1+j\tau_{ii}\omega)}\zeta}{2}\right)} \right) \left(\frac{1}{1+j\sigma_e\Lambda_{0,ii}^2\mu\omega}\right)\mu \quad (33)$$

The low pass filtering behaviour of the apparent magnetic permeability with time harmonics is well described by the model (see Figure 9). Eddy currents damping can come from the magnetic domains' rotation (contribution of τ) or the walls motion (contribution of Λ^2). Comparison between simulations and experiments and with linear assumptions will be carried out in the next section. The aim is to be able to fit the experimental data in most of the situations (geometry, polarisation magnitude, frequency), and this partly thanks to the intrinsic parameters κ (static flux dependent contribution) and the changeable one $[\Lambda_{surf}]=[\Lambda_0]$ (dynamic frequency dependent contribution) making involved the geometry dependent effects. Without changing neither the material (κ) nor the surface property Λ_0, the cut frequency would be unchanged (but just the module) with the thickness ζ (see Figure 17, [21]). This agrees with experiments (see next section), but varying ζ might in most of the cases imply a change in Λ_0 as well (see Figure 9). Finally, an increase in ζ provokes a decrease in $|\mu_{app,1}/\mu|$, whereas it stimulates an increase for $|\mu_{app,2}/\mu|$, certainly because of more space in favour of the disoriented.

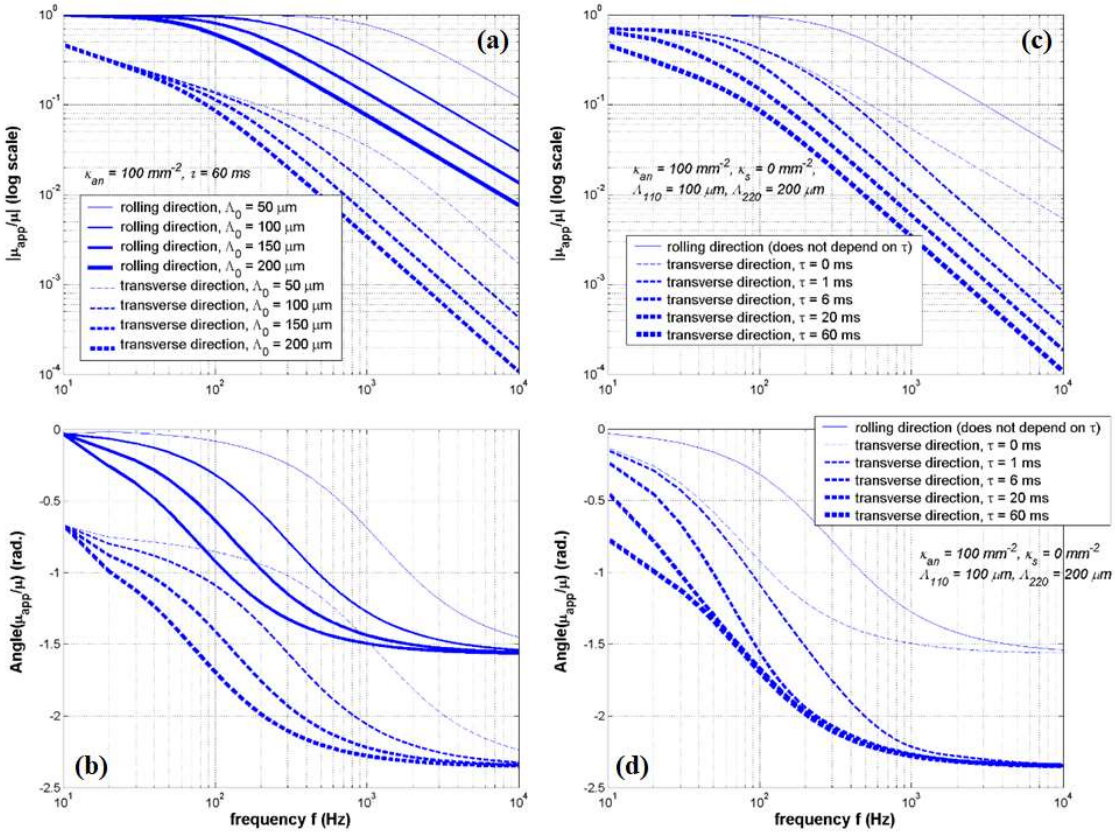

Figure 9: Sensitivity analysis of dynamic apparent permeability to the surface magnetic structure ((a) magnitude and (b) phase) and to the damping time delay ((c) magnitude and (d) phase angle)

6.2.3. Frequency dependent magnetic losses

The general definition of the mean power loss density for any periodic signal is given by (24). For time harmonics, the corresponding energy $<<\xi>_r>_t$ per cycle and per Tesla^2 becomes (34) then (in W.s.T^{-2}.kg^{-1} or J. T^{-2}.kg^{-1}). Underlined vectors are complex magnitudes and * means conjugation. In the general case, the dynamic quantity in (34) might include several contributions for each scalar product in each direction. It may however be possible to identify all the $\Lambda^2_{ij,0}$ by statistically separating every component and by using additional internal relationships and connections within $[\Lambda_0^2]$ factors. We now give an example for which there are two contributions in two directions only and choosing a complex coercive reluctivity $j\nu_c$. The Figure 10 shows that the total iron losses at frequencies up to the quasi-static conditions ($f > 10$ Hz) are driven mainly by the dynamic losses that can only increase with the frequency (eddy currents losses around walls and inside the domains). The results of Figure 10 are in accordance with expected average behaviour of energy losses versus the frequency ($f=\omega/(2\pi)$) and the geometry (ζ). The latter also show the impact of Λ_0, κ_s and τ, but varying only one parameter at a time. It is often hard to distinguish the true origins of experimental loss variations (§ 7) because several parameters can vary at the same time.

$$\ll \xi >_r>_t = \frac{\pi \ll p >_r>_t}{d\omega \left|< \vec{J} >_r\right|^2} = \ll \xi_{stat} >_r>_t + \ll \xi_{dyn} >_r>_t$$

$$<<\xi_{dyn}>_r>_t = +\mathrm{Re}\left(\frac{\pi\sigma\left[\Lambda_{surf}^2\right]\omega\vec{\underline{J}}_{surf}<\vec{\underline{J}}>_r^*}{d\left|<\vec{\underline{J}}>_r\right|^2}\right)=\sum_i \xi_{di}$$

$$\xi_{di}=\frac{\pi\sigma_e\Lambda_{0,ii}^2\omega}{d}\,\mathrm{real}\left(\frac{\left(1+j\sigma_e\Lambda_{0,ii}^2\mu\omega\right)\left(\frac{\sqrt{\kappa_{ii}(1+j\tau_{ii}\omega)}\zeta}{2}\right)}{\tanh\left(\frac{\sqrt{\kappa_{ii}(1+j\tau_{ii}\omega)}\zeta}{2}\right)}\right) \quad (34)$$

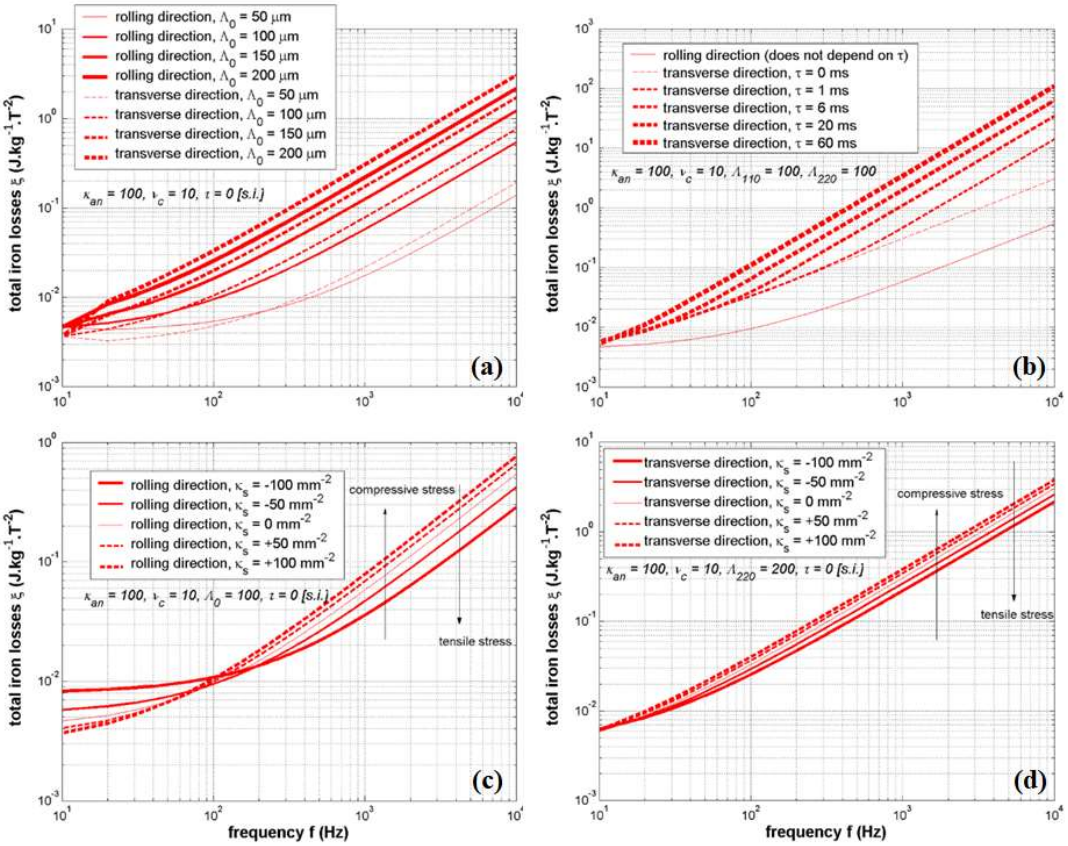

Figure 10: Sensitivity analysis of losses to the surface magnetic structure (a) , to the eddy currents time delay (b) and to the stress anisotropy ((c) and (d)).

7. Experimental results and identification of GO SiFe steel properties

In this section, we identify the material properties of a GO SiFe thanks to sheet samples with various thicknesses and the Epstein frame. Quasi-static properties $\kappa(B,\zeta)$ and $\nu_c(B,\zeta)$ can be determined with the static losses $<<\xi_{stat}>_r>_t$ and permeability $|\mu_{app}/\mu|$ when $\omega=2\pi f$ tends towards 0; whereas dynamic properties $\Lambda_0(B,f,\zeta)$ and $\tau(B,f,\zeta)$ are found thanks to the frequency dependent dynamic losses $<<\xi_{dyn}>_r>_t$ and apparent permeability $|\mu_{app}/\mu|$. In the whole results below, we can estimate the maximum inaccuracies that mainly depend on the current I and voltage V measured as follows:

$$\delta I=(\pm 2\pm 1\%\mathrm{I})[\mathrm{mA}];\ \delta V=(\pm 6.5\pm 1\%\mathrm{V})[\mathrm{mV}]$$

$$\Rightarrow \delta H=(\pm 1\pm 2\%\mathrm{H})[\mathrm{A/m}];\ \delta(\mathrm{fB})=\left(\pm 0.21\pm 2\%(\mathrm{fB})\right)[\mathrm{T.Hz}]$$

$$\delta(\mathrm{fB}^2\xi)=\left(\pm 0.1\pm 3\%(\mathrm{fB}^2\xi)\right)[\mathrm{mW/kg}];\ \delta\left(\mathrm{f}\mu_{app}/\mu_0\right)=\left(\pm 26000\pm 4\%\left(\mathrm{f}\mu_{app}/\mu_0\right)\right)[\mathrm{Hz}]$$

$$\Rightarrow \delta(\mathrm{fB}^2\nu_c)=\left(\pm 0.25\pm 3\%(\mathrm{fB}^2\nu_c)\right)[\mathrm{W/m^3}];\ \delta\kappa/\kappa=\pm 5\%;\ \delta(\mathrm{fB}\Lambda_0)=\left(\pm 132\pm 3\%(\mathrm{fB}\Lambda_0)\right)[\mathrm{T.Hz.\mu m}];\ \delta\tau/\tau=\pm 5\%$$

7.1. The samples

Epstein samples (with dimensions 30*300 mm^2) with a stress releasing annealing after cutting were used. Measurements were carried out on four thicknesses (ζ = 0.23 / 0.27 / 0.30 / 0.35 mm) starting from the same initial material composition (SiFe with 3% of Si). The volume mass density of this GO steel is 7650 kg.m^{-3} and its electrical resistivity 48 µΩ.cm. The manufacturing processes are adapted for the whole samples in order to make disappear any significant differences in terms of typical grains' dimension (5-35 mm), orientation (6° max disorientation), coating material (Inorganic based divided in two layers, one layer of glass-film and one layer of phosphated insulator) and coating thickness (2-4 µm) and its thermal curing temperature (T>800°C, few minutes).

7.2. Quasi-static equilibrium

7.2.1. Static apparent permeability

7.2.1.1. Mesoscopic anisotropy constant

Considering the same material used for the samples with different thicknesses, it is reasonably assumed that the properties μ, σ_e and κ_{an} are the same for the whole samples. This can be confirmed for μ by studies done in [27]. Thus, we propose to explain the differences observed on the apparent magnetic permeability for the four thicknesses (see Figure 12) by the self-magnetostriction and stress induced anisotropy described by the property κ_s (see Figure 11). We think that a manufacturing tensile residual stress due to the rolling and coating processes corresponds to a negative property $\kappa_s<0$ at low induction. For higher induction, the material's self-magnetostriction increases with the magnetization, it corresponds to an equivalent induced compressive stress that becomes bigger than the tensile residual stress effect. Even if the rolling and coating processes are approximately the same for the four thicknesses, it seems that the thinner the sheet, the bigger the residual and magneto-strictive induced stresses. Figure 11 Shows the property κ_s identifications relative to the property κ_s of the material with thickness $\zeta = 0.35$ mm.

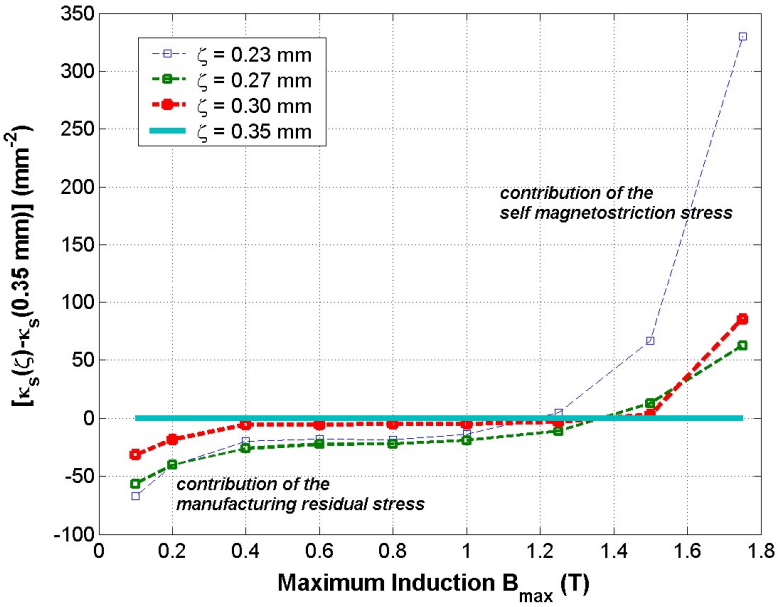

Figure 11: Experimental identification of κ_s, *i.e.* the product magneto-crystalline anisotropy * magnetostriction anisotropy over the squared exchange energy.

7.2.1.2. Stress sensitive static apparent permeability

Figure 12 gives the quasi-static apparent magnetic permeability of each thickness relative to the thickness $\zeta = 0.35$ mm. Considering the corresponding identification of κ_s (see Figure 11); the data obtained by the calculation fit exactly the data measured with no discrepancy.

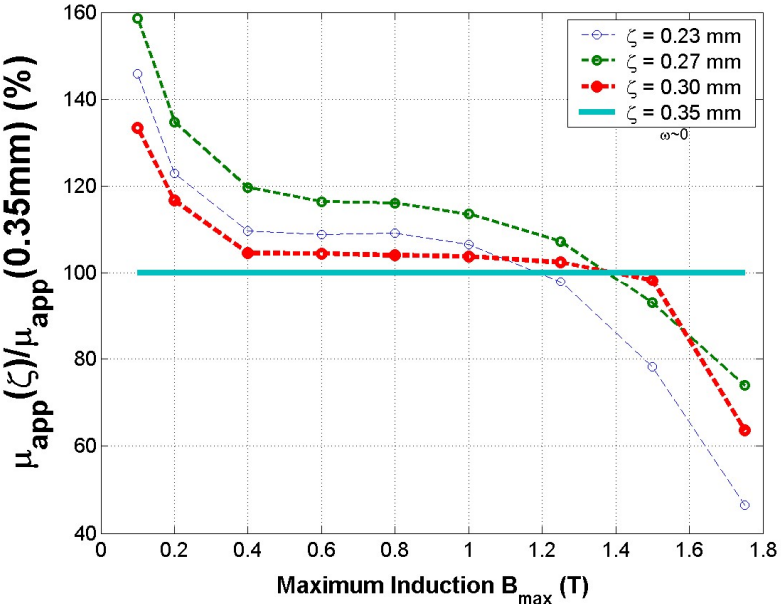

Figure 12: Magnetostriction and stress sensitive quasi-static apparent permeability (measured and calculated).

7.2.2. Magnetic losses

7.2.2.1. Coercive force reluctivity

The coercive loss reluctivity ν_c defined by (18), (24) and (32) corresponds to the hysteresis loss coefficient K_h of Bertotti [23]. This coefficient has been identified in Figure 13 for the four thicknesses of GO SiFe sheet with the help of the quasi-static hysteresis loss measured at varying maximum induction B_{max}. As shown in Figure 13 the property depends on B_{max}. At low induction, *i.e.* in the Rayleigh zone, the ν_c is relatively high and at is maximum for the thickness $\zeta = 0.35$ mm. In this area, the magnetic walls are easily pinned and bowed by the defects and these effects are increasing when the thickness of grains and walls increase. It is coherent with a low static permeability of the first magnetization curve. Then ν_c decreases for medium induction, which might correspond to an increase of the quasi-static permeability towards its maximum value. At higher induction, ν_c increases again, probably due to higher field necessary to activate, nucleate and multiply the walls from one polarization to the other direction. This time, it is inside the thickest sheets that it seems easier to nucleate and activate the walls. Thus, at high induction level, the thinner the sample the higher the coercive loss reluctivity ν_c.

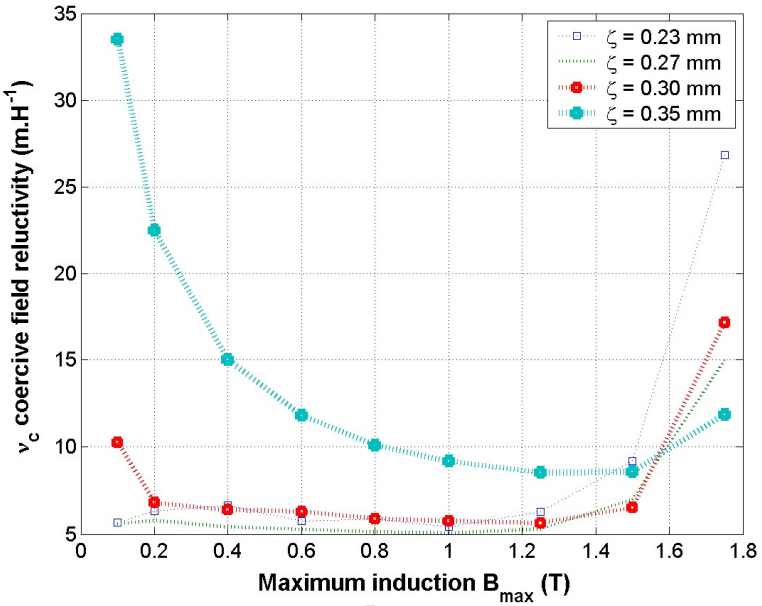

Figure 13: Experimental identification of ν_c, *i.e.* the Ratio between the coercive loss field and the flux density as a function of the induction level.

7.2.2.2. Coercivity dependent static losses

Quasi-static measurements have been carried out at low frequency f = 10 Hz for which the skin depth ($\delta \sim 0.8$ mm) is very high compared to the biggest thickness. Figure 14 gives the quasi-static hysteresis losses of each thickness. Considering the corresponding identification of ν_c (see Figure 13); the data obtained by the calculation fit exactly the data measured with no discrepancy. However, no correlation can be proposed for these results. Even though the four thicknesses have got different coercive loss reluctivity, the hysteresis loss per unit mass and per squared induction of the four thicknesses are approximately the same and far below the dynamic losses up to 50 Hz.

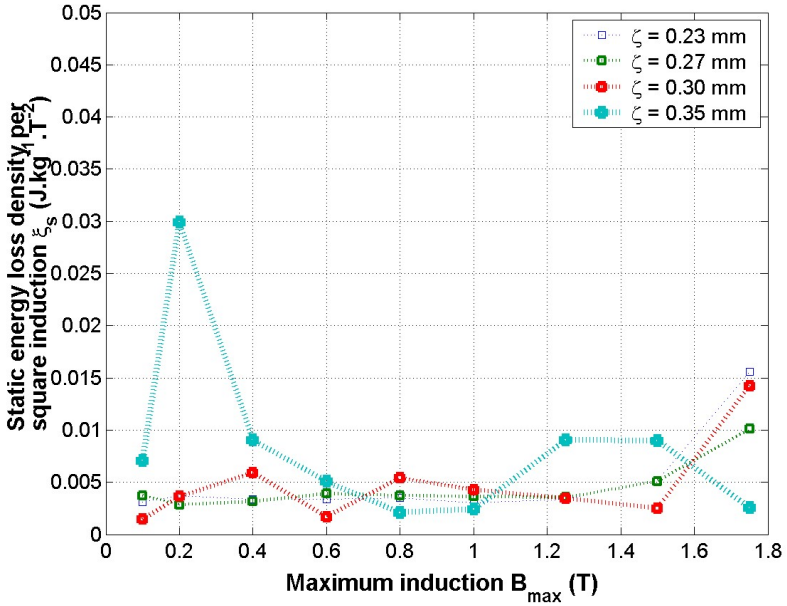

Figure 14: Quasi static losses of the four samples with four thicknesses as a function of the induction level (measured and calculated)

7.3. Frequency dependent dynamic magnetization

7.3.1. Dynamic properties

The coupled dynamic properties $\Lambda_0(B,f,\zeta)$ and $\tau(B,f,\zeta)$ are found simultaneously thanks to the frequency dependent dynamic losses $\langle\langle\xi_{dyn}\rangle_r\rangle_t$ and apparent permeability $|\mu_{app}/\mu|$ together. Measurements have been carried out from 10 to 600 Hz and the whole induction levels. However, accuracy up to 300 Hz is low and only measurements at low induction are exploited to limit any non-linearities.

7.3.1.1. Volume diffusion time due to eddy currents

Figure 15 gives the identification of the volume diffusion time τ, also called the damping field time delay or the eddy currents time delay. As expected, the diffusion time increases when the thickness increases for frequency up to 30 Hz. Microscopic eddy currents time delay increases for domains and wall with bigger dimensions. A domains refinement effect is noticed (Figure 16) for increasing frequency. It seems logical to have then a decreasing τ. Microscopic eddy currents time delay decreases for domains and walls with smaller dimensions.

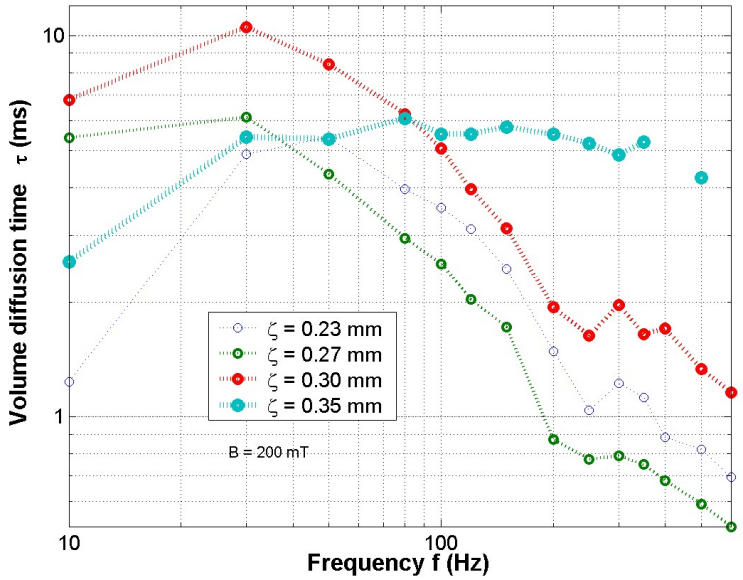

Figure 15: Experimental identification of the volume diffusion time, or the eddy currents time delay, $\tau \alpha \sigma\mu/Ks$ @0.2 T.

7.3.1.2. Surface magnetic structure

Figure 16 shows identifications of the surface structure property $\Lambda_0 = \Lambda_{110}$ in the rolling direction. For all thicknesses, we notice a domains refinement effect when increasing the frequency, probably due to magnetic walls bowing and multiplication.

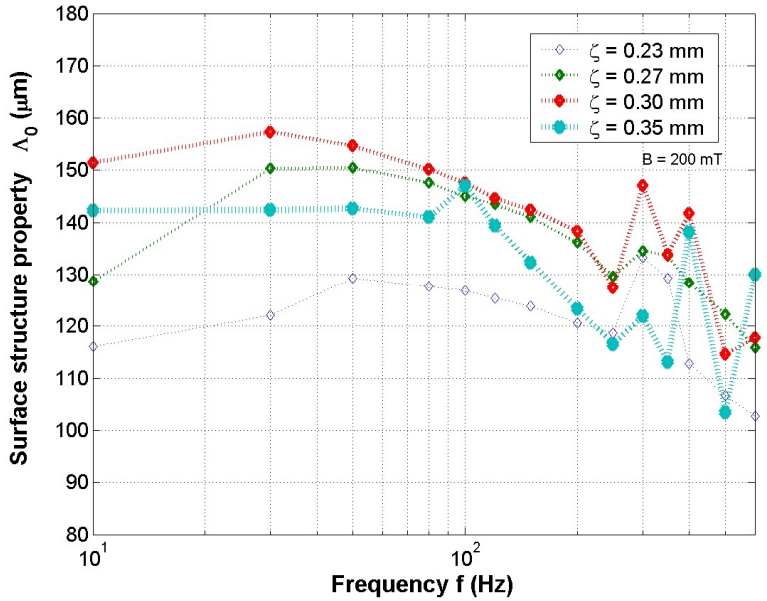

Figure 16: Experimental identification of the surface dynamic property $\Lambda_0 = \Lambda_{110}$ in the rolling direction @0.2 T.

7.3.2. Dynamic observables

7.3.2.1. Dynamic apparent permeability

Apparent permeability measurements have been carried out at various frequencies. Figure 17 gives the results for each thickness. Considering the corresponding identification of τ and Λ_0 (see Figure 15 and Figure 16); the data obtained by the calculation fit exactly the data measured with no discrepancy. As expected, the magnetic behaviour is a low pass filter and the permeability magnitude decreases with both the frequency and the thickness. However, no variation of the cut frequency is noticeable.

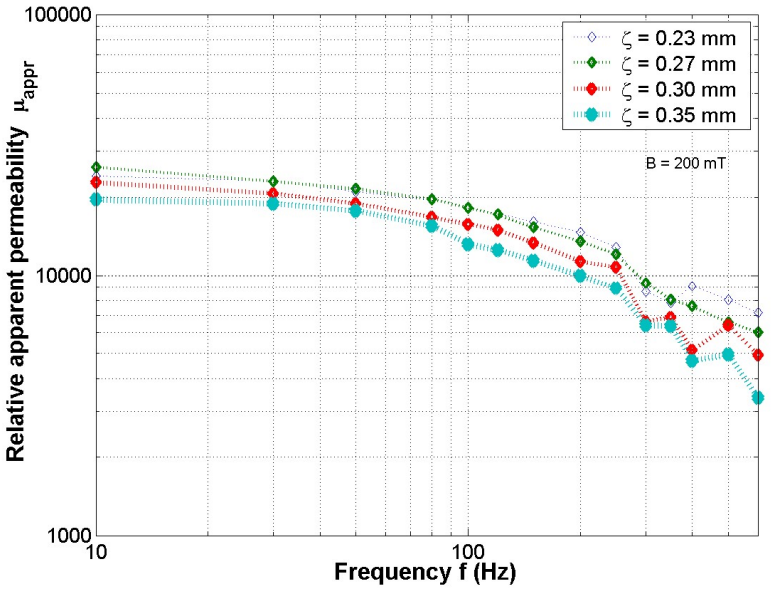

Figure 17: Dynamic frequency dependent apparent permeability (measured and calculated)

7.3.2.2. Magnetic losses

Total and dynamic loss measurements have been carried out at various frequencies. Figure 18 gives the results for each thickness. Considering the corresponding identification of τ and Λ_0 (see Figure 15 and Figure 16); the data obtained by the calculation fit exactly the data measured with no discrepancy. As expected, the losses increase with both the frequency and the thickness. The type of variations will depend on the frequency dependent properties τ and Λ_0. This effect corresponds to the power law of the excess loss by Bertotti [23].

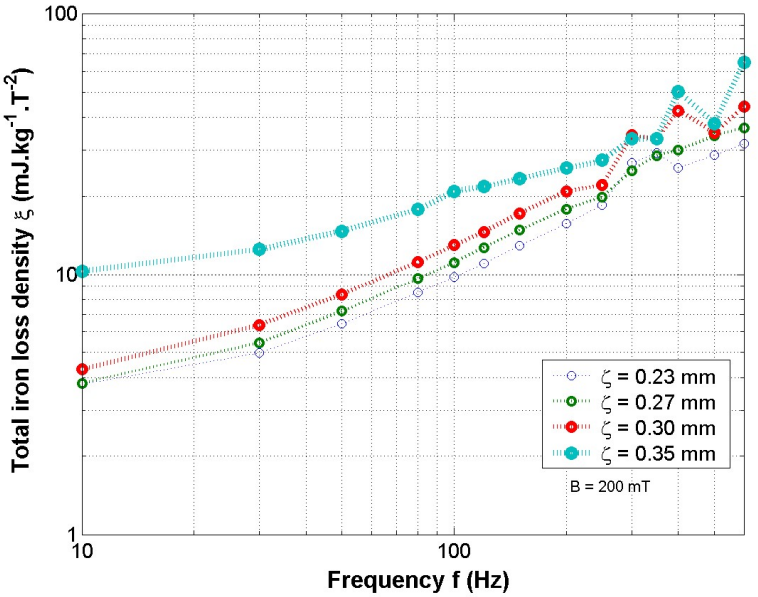

Figure 18: Total frequency dependent losses (measured and calculated)

7.4. Discussions

Providing some boundary conditions on the surface magnetic structure ($[\Lambda_0^2]$), it is possible to deduce its variations everywhere else in the material, whatever its geometry is. Knowing all this information and considering also static and dynamic phenomena, such as hysteresis, walls

motion and magnetic domains' rotation, computing the heterogeneous magnetic structuring and the geometry and frequency dependent vector magnetic behaviour and losses becomes possible. To do so, it is however necessary to know the value of some usual materials' properties: the electrical conductivity (σ_e) and the quasi-static permeability (μ); and to define new properties: the coercive loss reluctivity (ν_c), the macroscopic anisotropy coefficients (either magneto-crystalline κ_{an}, magneto-strictive or/and stress induced κ_s) and the volume diffusion time delay (τ). Nevertheless, experimental identifications can provide us the required values of all these material parameters. The model and the methodology have been checked with four thicknesses of GO SiFe sheet samples, mainly in the rolling direction. It would require more calculations and measurements thanks to more samples to validate the complete model in the whole directions. In fact, any identification of every material parameters can only be done with several geometries, flux density orientations, levels and frequencies. The formulation can be viewed at present for macroscopic polycrystalline materials only. It reproduces the dependence of magnetic domains structures and losses with the geometry.

8. Conclusion and forthcoming

As a conclusion, the tensor magnetic phase theory is a deterministic but energetic and statistical theory to predict space and time variations of the domains' and walls' organisation and properties everywhere in a soft magnetic material, whatever its geometry is. The present model does not make any arbitrary assumption concerning the type and topology of domains. It can also take complex domains shapes statistically into account, thanks to its cross-sectional areas and its walls mobility and density. Thus, this method is no more confronted to serious limitations due to the huge number of degrees of freedom, considering the infinite variety of magnetic structures. The latter might be statistically described thanks to the infinite possible values of the 6 independent terms present in $[\Lambda^2]$. However, it does not always allow to separate from the domains' and walls' size effects and their rotation and mobility effects. It can make sense only for large enough specimens, *i.e.* that contain numerous enough domains to be statistically representative. For a steel sheet, the width and the length should be very large compared to Λ. The tensor magnetic phase theory is based on structural magnetic domains and walls, but statistical state variables have been investigated assuming known the quasi static permeability μ and static hysteresis and coercive field $\nu_c B$. It also takes the grains, grains size and grains boundaries in the macroscopic anisotropy κ_{an} into account. It includes the self-magnetostriction anisotropy $\kappa_{\lambda\varepsilon}$ and stress-induced anisotropy $\kappa_{\lambda\sigma}$ as well. The exchange and anisotropy energy density of walls γ_w being involved in the definition of all these macroscopic anisotropy properties (κ_{an}, $\kappa_{\lambda\varepsilon}$, $\kappa_{\lambda\sigma}$). Evolutions of the magnetic structure in time does not occur instantaneously but with a time delay τ that is depends on the volume microscopic eddy currents around walls and inside domains that damp the walls' motion and the domains' magnetic rotation. Finally, the volume magnetic structure is significantly influenced by the surface limit conditions, and it cannot be determined without this condition. The latter limit condition involves a coupling to the external magnetic field through a dynamic magnetic behavioral law, that makes the connection between the field and the surface magnetic polarization. In this coupling between the magnetic field and the magnetic structure, the surface structural property $[\Lambda_0^2]$ has got an essential role to play. At present, this surface property is considered as a model parameter to be identified with measurements, like the seven main parameters of the model (σ_e, μ, ν_c, κ_{an}, $\kappa_{\lambda\varepsilon}$, $\kappa_{\lambda\sigma}$, τ). In the near future, we think that this new model can help us study and optimize the impact of any surface treatments (coating, scratching, scribing, irradiation …) and especially the surface laser treatments (laser irradiation, scribing, ablation, laser induced shock wave, laser induced polarized sub-structure …) with different patterns on the magnetic structure with domains and walls. This goal will be achievable only if further investigations are carried out to develop the surface minimization principle (see surface integral of (12)) in addition to the present volume magnetic structure model. Determination of optimal surface treatments' parameters and patterns may be possible by inversing the model and defining its goal criteria.

Bibliography

[1] M-A. Raulet, B. Ducharne, J-P. Masson, and G. Bayada, "The magnetic field diffusion equation including dynamic hysteresis", *IEEE Transactions on Magnetics*, 2004, vol. 42, n°2, pp. 872–875.

[2] O. Maloberti, V. Mazauric, G. Meunier, A. Kedous-Lebouc, O. Geoffroy, "An Energy-Based Formulation for Dynamic Hysteresis and Extra-Losses", *IEEE Transactions on Magnetics*, 2006, vol. 42, n°4, pp. 895-898.

[3] A. Hubert, R. Schafer, *Magnetic Domains*, Springer Verlag, 2000.

[4] D.H. Martin, "Surface Structures and Ferromagnetic Domain sizes", *Proc. Phys. Soc.*, 1956, vol. 70, pp. 77-84.

[5] Y. A. S. Shur, YU. N. Dragoshanskiy, "The shape of closure domains inside silicon iron crystals", *Fiz. Metal. Metalloved*, 1966, vol. 22, n°5, pp. 702-710.

[6] L. Néel, "Les lois de l'aimantation et de la subdivision en domaines élémentaires d'un monocrystal de Fer", *Journal de Physique et le Radium*, 1944, Tome 5, série 8(11), pp. 241-251.

[7] C. Kittel, "Physical Theory of Ferromagnetic Domains", *Reviews of Modern Physics*, 1949, vol. 21, n°4, pp. 541-583.

[8] G. Bertotti, *Hysteresis in Magnetism*, Academic Press, 1998, pp. 391-430, pp. 129-162.

[9] G. Lochak, *La Géométrisation de la Physique*, Flammarion, 1994.

[10] O. Maloberti, A. Kedous-Lebouc, O. Geoffroy, G. Meunier, and V. Mazauric, "Field Diffusion-Like Representation and Experimental Identification of a Dynamic Magnetization Property", *Journal of Magnetism and Magnetic Materials*, 2006, vol. 304, pp. e507-e509.

[11] O. Maloberti, *Contribution à la Modélisation des Effets Dynamiques dans les Matériaux Magnétiques Doux : Caractérisation et Simulation*, PhD ed. EEATS/INPG Grenoble, Septembre 2006.

[12] H.A.M. Van Den Berg, A.H.J.V.D. Brandt, "Self-Consistent Domain Theory in Soft Ferromagnetic Media II: Basic domains structures in thin film objects", *Journal of Applied Physics*, 1986, vol. 60, n°3, pp. 1105-1113.

[13] H.A.M. Van Den Berg, A.H.J.V.D. Brandt, "Self-Consistent Domain Theory in Soft Ferromagnetic Media III: Composite domains structures in thin film objects", *Journal of Applied Physics*, 1987, vol. 62, n°5, pp. 1952-1959.

[14] A. De Simone, "Energy Minimizers for Large Ferromagnetic Bodies", *Arch. Rat. Mech. Anal.*, 1993, vol. 125, pp. 99-143.

[15] J. Hladik, P.E. Hladik, *Le Calcul Tensoriel en Physique*, Dunod 3rd ed., Paris, 1999.

[16] E.A. Wood, *Crystals and Light*, Dover Pub. Inc., New York, 1977.

[17] M.I. Darby, E.D. Isaac, "Magnetocrystalline Anisotropy of Ferro- and Ferrimagnetics", *IEEE Transactions on Magnetics*, June 1974, vol. MAG-10, n°2, pp. 259-299.

[18] T.L. Gilbert, "A Phenomenological Theory of Damping in Ferromagnetic Materials", *IEEE Transactions on Magnetics*, November 2004, vol. 40, n°6, pp. 3443-3449.

[19] J.B. Passioura, "Simulation Models: Science, Snake-Oils, Education or Engineering", *Agronomy Journal*, 1996, vol. 88, pp. 690-694.

[20] O. Maloberti, G. Meunier, A. Kedous-Lebouc, V. Mazauric, "How to Formulate Soft Materials Heterogeneity? *1. Quasi-Static Equilibrium and Structuring*", Conference SMM'18 in Cardiff 2007.

[21] O. Maloberti, A. Kedous-Lebouc, G. Meunier, V. Mazauric, "How to Formulate Soft Materials Heterogeneity? 2. Hysteresis, Dynamic Motions and Diffusion", Conference SMM'18 in Cardiff 2007.

[22] J.W. Shilling, G.L. Houze, "Magnetic Properties and Domain Structure in Grain-Oriented 3 % Si-Fe", *IEEE Transactions on Magnetism and Magnetic Materials*, 2006, volume Mag-10, no 2, pp. 223.
[23] G. Bertotti, "General Properties of Power Losses in Soft Ferromagnetic Materials", *IEEE Transactions on Magnetics*, 1980, vol. 24(1), pp. 621-630.
[24] D.C. Jiles, D.L. Atherton, "Theory of Ferromagnetic hysteresis", *Journal of magnetism and Magnetic Materials*, 1986, vol. 61, pp. 48-60.
[25] N. Buiron, « Modélisation multi-échelle du comportement magnéto-élastique couplé des ferromagnétiques doux », PhD thesis, Ecole Normale Supérieure de Cachan, Department of Mechanics, 2000.
[26] H. Williams, W. Shockley, C. Kittel, "Studies of the propagation velocity of a ferromagnetic domain boundary", Physical Review, 1950, vol. 80, n°6, pp. 1090-1094.
[27] O. Maloberti et al., "Testing the sheet thickness dependence of a dynamic magnetization property based on domains and walls within the diffusion-like equation for GO SiFe", *2DM conference*, Grenoble, 2018.

Acknowledgments

Samples with a stress relieving treatment were kindly given by TKES (ThyssenKrupp Electrical Steels). Measurements were carried out by the LSEE (Laboratoire des Systèmes Electrotechniques et Environnement) and the UNILASALLE Amiens (ESIEE Amiens). Modeling and identification researches were performed at the UNILASALLE Amiens (ESIEE Amiens) and has received funding from the European Research Council under the European Union's H2020-IND-CE-2016-17/H2020-FOF-2017 Program (Grant Agreement No. 766437).

Appendix: Mathematical tools

Operators

$[Y] = \left[\vec{Y}_1, \vec{Y}_2, \vec{Y}_3\right] = \begin{bmatrix} Y_{11} & Y_{12} & Y_{13} \\ Y_{21} & Y_{22} & Y_{23} \\ Y_{31} & Y_{32} & Y_{33} \end{bmatrix}$, $[n] = [\vec{n}, \vec{n}, \vec{n}]$: $[Y]^T$ means to transpose the matrix $[Y]$

$[\vec{\nabla}](\vec{A}) = [\vec{\nabla} \otimes \vec{A}], \left[[\vec{\nabla}](\vec{A})\right]_{ij} = [\vec{\nabla} \otimes \vec{A}]_{ij}$: tensor gradient on a vector,

$\vec{\nabla} \cdot [Y] = \left(\vec{\nabla} \cdot \vec{Y}_1, \vec{\nabla} \cdot \vec{Y}_2, \vec{\nabla} \cdot \vec{Y}_3\right)^T$: vector divergence on a tensor,

$[\vec{\nabla}] \times [Y] = [\vec{\nabla} \times][Y] = \left[\vec{\nabla} \times \vec{Y}_1, \vec{\nabla} \times \vec{Y}_2, \vec{\nabla} \times \vec{Y}_3\right]^T$: tensor rotational on a tensor,

$[\Delta][Y] = \left[\vec{\Delta}(\vec{Y}_1), \vec{\Delta}(\vec{Y}_2), \vec{\Delta}(\vec{Y}_3)\right]^T$: tensor Laplacian on a tensor,

$\vec{\nabla} \cdot = (\partial_1 \cdot, \partial_2 \cdot, \partial_3 \cdot)^T$: Nabla operator,

$\vec{\Delta} \cdot = (\partial_1\partial_1 \cdot, \partial_2\partial_2 \cdot, \partial_3\partial_3 \cdot)^T$: Laplacian operator

Operations

$[\vec{A} \otimes \vec{B}], [\vec{A} \otimes \vec{B}]_{ij} = A_i B_j$: tensor product between two vectors.

$[[Y] \cdot\cdot [Z]], [[Y] \cdot\cdot [Z]]_{ij} = Y_{ij} Z_{ij}$: tensor product type 1 between 2 tensors.

$[[Y] \times [Z]] = \left[\vec{Y}_1 \times \vec{Z}_1, \vec{Y}_2 \times \vec{Z}_2, \vec{Y}_3 \times \vec{Z}_3\right]^T$: tensor product type 2 between 2 tensors.

$([Y] \overrightarrow{\odot} [Z]) = \left(\vec{Y}_1 \cdot \vec{Z}_1, \vec{Y}_2 \cdot \vec{Z}_2, \vec{Y}_3 \cdot \vec{Z}_3\right)^T, \left([Y] \overrightarrow{\odot^2}\right) = ([Y] \overrightarrow{\odot} [Y])$: vector product between 2 tensors.

$[Y] \circ [Z] = Y_{ij} Z_{ij}$: scalar product between two tensors.

Derivative and integral properties

$[\vec{\nabla} \times][\vec{\nabla} \times][Y] = [\vec{\nabla}](\vec{\nabla} \cdot [Y]) - [\Delta][Y]$

$[X] \overrightarrow{\odot} ([Y] \times [Z]) = [Z] \overrightarrow{\odot} ([X] \times [Y]) = [Y] \overrightarrow{\odot} ([Z] \times [X])$

$\vec{\nabla} \cdot ([Y]\vec{A}) = (\vec{\nabla} \cdot [Y]) \cdot \vec{A} + [Y] \circ [\vec{\nabla} \otimes \vec{A}]$

$$\iint_{\Omega} (\vec{\nabla} \cdot \vec{A})\, d^3x = \oiint_{\partial\Omega} (\vec{A} \cdot \vec{n}) d^2x$$

$$\iint_{\Omega} (\vec{\nabla} \times \vec{A})\, d^3x = \oiint_{\partial\Omega} -(\vec{A} \times \vec{n}) d^2x$$

$$\iint_{\Omega} (\vec{\nabla} \cdot [Y])\, d^3x = \oiint_{\partial\Omega} ([Y] \overrightarrow{\odot} [n]) d^2x$$

$$\iint_{\Omega} ([\vec{\nabla}] \times [Y])\, d^3x = \oiint_{\partial\Omega} -([Y] \times [n]) d^2x$$

$$\iint_{\Sigma} ([\vec{\nabla}] \times [Y])\, d^2x = \oint_{\partial\Sigma} ([Y] \overrightarrow{\odot} [n])\ dx$$